Submitted version June 28, 2002

The Palomar/MSU Nearby Star Spectroscopic Survey IV: The Luminosity Function in the Solar Neighbourhood and M Dwarf Kinematics [1]

I. Neill Reid

Space Telescope Science Institute, 3700 San Marin Drive, Baltimore, MD 21218
and
Department of Physics and Astronomy, University of Pennsylvania, 209 South 33rd Street, Philadelphia PA 19104-6396

inr@stsci.edu

John E. Gizis

Department of Physics & Astronomy, University of Delaware

gizis@udel.edu

Suzanne L. Hawley

Astronomy Dept, Box 351580, Univ of Washington, Seattle, WA 98195

slh@pillan.astro.washington.edu

ABSTRACT

We have used new astrometric and spectroscopic observations to refine the volume-complete sample of M dwarfs defined in previous papers in this series. With the addition of Hipparcos astrometry, our revised VC[2] sample includes 558 main-sequence stars in 448 systems. Analysis of that dataset shows no evidence for any systematic kinematic bias. Combining those data with an Hipparcos-based sample of AFGK dwarfs within 25 parsecs of the Sun, we have derived the Solar Neighbourhood luminosity function, $\Phi(M_V)$, for stars with absolute magnitudes between -1 and +17. Using empirical and semi-empirical mass-M_V relations, we transform $\Phi(M_V)$ to the present-day mass function, $\psi(M)$ ($\frac{dN}{dM}$). Depending on the mass-luminosity calibration adopted, $\psi(M)$ can be represented by either a two-component or three-component power-law. In either case, the

power-law index, α, has a value of ~ 1.3 at low masses ($0.1 < \frac{M}{M_\odot} < 0.7$), and the local mass density of main sequence stars is $\sim 0.031 M_\odot pc^{-3}$.
We have converted $\psi(M)$ to an estimate of the initial mass function, $\Psi(M)$, by allowing for stellar evolution, the density law perpendicular to the Plane and the local mix of stellar populations. The results give $\alpha = 1.1$ to 1.3 at low masses, and $\alpha = 2.5$ to 2.8 at high masses, with the change in slope lying between 0.7 and $1.1 M_\odot$.
Finally, the (U, W) velocity distributions of both the VC[2] sample and the fainter ($M_V > 4$) stars in the Hipparcos 25-pc sample are well-represented by two-component Gaussian distributions, with ∼10% of the stars in the higher velocity-dispersion component. We suggest that the latter component is the thick disk, and offer a possible explanation for the relatively low velocity dispersions shown by ultracool dwarfs.

Subject headings: (Galaxy:) solar neighborhood — stars: kinematics — stars: luminosity function, mass function

1. Introduction

The nearest stars represent an important tool in studies of Galactic structure, since they provide an opportunity for detailed analysis of constituent members of the various stellar populations and sub-populations. This holds particularly for M dwarfs, which account for the overwhelming majority of stars currently present in the Galaxy. With a local density of ~ 0.07 pc^{-3}, these stars are ideal tracers of many properties of the Galactic disk. Until recently, the main limitation in such analyses was the lack of basic observational data, such as spectral types or radial velocities. Our main goal in undertaking the Palomar/Michigan State University (PMSU) survey (Reid, Hawley & Gizis, 1995, PMSU1; Hawley, Gizis & Reid, 1996, PMSU2; Hawley, Gizis & Reid, 1997), was to remedy this defect by compiling moderate resolution spectroscopy for all M dwarfs in the preliminary version of the third Catalogue of Nearby Stars (Gliese & Jahreiß, 1991; pCNS3). We obtained observation of over 2000 candidate M dwarfs, omitting only unresolved binary companions. Calculating distances by combining spectroscopic parallaxes with the then-available trigonometric data, we defined M_V-dependent distance limits which isolate a volume-complete sample, and used

[1]Based partly on observations made at the 60-inch telescope at Palomar Mountain which is jointly owned by the California Institute of Technology and the Carnegie Institution of Washington

that sample to derive estimates of the luminosity function and the velocity distribution of low mass stars (PMSU1), in addition to studying the range of chromospheric activity (PMSU2).

Since the completion of our initial analysis, two major new datasets have become available. First, the Hipparcos catalogue has been published (ESA, 1997), including milliarcsecond-accuracy astrometry for over 110,000 stars brighter than 13th magnitude. Almost two-thirds of the stars in the pCNS3 have observations by Hipparcos. Second, as a follow-up to PMSU, we obtained echelle spectroscopy of many of the brighter M dwarfs in the pCNS3, including all of the stars in the volume-complete sample defined in PMSU1. Those data are now fully analysed, and presented by Gizis, Reid & Hawley (2002; PMSU3). The high-resolution observations provide significantly more accurate radial velocities, besides more sensitive measurement of chromospheric activity.

Both of these new datasets have potential importance for the results of the analysis presented in PMSU1. Revising the distances of a substantial number of stars affects both the composition of the volume-complete sample and the derived tangential motions, while the new radial velocity determinations affect the space motion determinations. We have therefore re-analysed the PMSU dataset, incorporating the new observational data. Section 2 describes the definition of the revised volume-complete sample; section 3 considers the effect on the luminosity function; section 4 rederives the mass function for nearby stars, combining our data with an Hipparcos 25-parsec sample of earlier-type main-sequence stars; and section 5 re-analyses the kinematics. The main results are summarised and discussed in section 6.

2. A volume-complete sample of Solar Neighbourhood M dwarfs

In PMSU1, we used the available trigonometric and photometric parallax information, together with our own distance estimates based on the (M_V, TiO5) calibration, to construct a volume-complete (VC) subset of the M dwarfs in the pCNS3. Over 2300 pCNS3 stars have Hipparcos astrometry, but, with incomplete sampling between V=8 and the Hipparcos limit of V=13, that dataset includes only 712 M dwarfs from PMSU1 and PMSU2. Coverage is better amongst the brighter stars in the PMSU1 VC subset, however, with data for 330 of the 499 systems.

Figure 1 compares pre- and post-Hipparcos distance measurements for PMSU stars; there is a systematic shift towards higher distances (parallaxes tend to be overestimated, hence the Lutz-Kelker bias), and a significant number of M dwarfs move beyond the 25 parsec boundary of the pCNS3. Seventy-one of the 499 systems in the VC sample have revised

distances which place the stars beyond the completeness limits adopted for the appropriate absolute magnitude. We have therefore re-analysed the pCNS3 dataset, augmented by new observations, and derive a revised volume-complete sample of M dwarfs, (VC^2).

2.1. Re-defining the sample

We have used the techniques described in PMSU1 to analyse the post-Hipparcos pCNS3 dataset, re-deriving the appropriate distance limits as a function of absolute magnitude. As before, we limit analysis to the 1684 M dwarf systems in the northern sample, $\delta > -30°$, and set absolute magnitude limits $8 \leq M_V \leq 16$. Figure 2 provides the justification for our choice of distance limits, plotting the run of density (ρ_{sys}, number of *systems* per unit volume) with increasing distance; the distance limits, d_{lim}, are set where ρ_{sys} flattens, before the downturn due to incompleteness. Applying Schmidt's (1968) V/V_{max} estimator to the same issue gives identical results.

As Table 1 shows, the revised distance limits match those derived in PMSU1, with the exception of the M_V=9.5 bin, where d_{lim} decreases by 10%. A total of 545 stars in 435 systems, including 300 with Hipparcos data, meet these distance criteria. This dataset includes additional companions identified by Reid & Gizis (1997, RG97), Delfosse *et al.* (1999) and Beuzit *et al.* (2001). Only 16 systems lack PMSU3 echelle observations, and the majority (381 systems) have distances derived from trigonometric parallaxes. The relevant data for each stellar system are listed in Table 2, where we also give the proper motions and space velocities.

Besides providing improved distance estimates for stars already known to lie within the immediate Solar Neighbourhood, Hipparcos also identified a number of previously-unrecognised nearby stars. The full catalogue lists 78 stars which are not in the pCNS3, but have $\pi_H > 45$ milliarcseconds (mas) or $r < 22$ parsecs. Of these, 23 have formal absolute magnitude values in the range $8 \leq M_V \leq 16$. Ten of the latter subset, however, have spectral types which are clearly inconsistent with the inferred absolute magnitude; for example, HIP 21000, or BD+4:701A, has $\pi_H = 84.8$ mas and an inferred $M_V = 9.5$, but spectral type F8. All ten are in binary systems, and the companion has influenced the astrometric results listed in the Hipparcos catalogue. This is a well known problem, which can be rectified through more sophisticated analysis; thus, Fabricius & Makarov (2000) derive $\pi_{H'} = 4.2$ mas for HIP 21000.

The remaining 13 stars in the supplementary sample are all confirmed M dwarfs. The parallax measurements for both Vyssotsky 130 (a double star) and HD 218422 have substan-

tial uncertainties. For the present, we retain both stars in the sample, increasing the revised VC[2] sample to 558 main-sequence stars[2] in 448 systems. Relevant data for the additional stars are listed in Table 3. With the exception of LHS 1234 (Weis, 1996), prior observations are scarce, and most lack radial velocity data. For those stars, the space motions listed in Table 3 are computed for $V_r = 0$ km s^{-1} .

2.2. Biases and completeness

A reliable determination of the properties of the local Galactic Disk demands an unbiased, representative stellar dataset. It is to that end that we constructed the VC[2] sample described in the previous section. However, while the $\rho(d)$ and $\frac{V}{V_{max}}(d)$ measurements show that the sample as a whole is broadly consistent with our requirements, subtle biases may remain, particularly since the stars are drawn primarily from a pre-existing catalogue (the pCNS3) rather than an unbiased all-sky survey. On the positive side, our VC[2] sample has the advantage that trigonometric parallax measurements are the dominant contributor to distance estimates for 90% of the systems. This is in contrast to the original PMSU1 VC sample, where 40% of the stars lacked accurate astrometry.

Two potential sources of bias are proximity to the Galactic Plane, where crowding might be a problem leading to omission of nearby stars; and proper motion-based selection, which could bias against nearby stars with low space motions. Considering the former issue, Figure 3 plots the distribution of the VC[2] sample on the celestial sphere. Based on the areal coverage, we expect 15.9% of the sample to lie within $\pm 10^\circ$ of the Galactic Plane; in fact, 69 of the 448 systems ($15.4 \pm 1.9\%$) lie within those limits. We conclude that crowding in the Galactic Plane is not a significant contributor to incompleteness in the VC[2] sample[3]

A greater concern is the potential for kinematic bias. As discussed in PMSU1 and PMSU2, most stars in the pCNS3 were identified based on their having high proper motion. Those stars are drawn predominantly from three major proper motion surveys: the Lowell survey, limited to $\mu > 0.26''$ yr^{-1} (Giclas, Burnham & Thomas, 1971); the Luyten Half Second catalogue (LHS), $\mu > 0.50''$ yr^{-1} , (Luyten 1979); and the New Luyten Two-Tenths Catalogue (NLTT), $\mu > 0.18''$ yr^{-1} , (Luyten, 1980). Those limits correspond to transverse

[2]There are an additional four white dwarf and three brown dwarf companions.

[3]We note that there *is* a statistically significant bias against low-latitude systems if we consider low luminosity stars in the full pCNS3: of the 395 stars north of -30° with with $M_V > 13$, only 41, or $10.4\% \pm 1.8\%$, lie within 10° of the plane. The distance and M_V limits imposed in defining the VC[2] sample have eliminated this potential source of bias.

velocities of, respectively, 24.6 km s^{-1} , 47.4 km s^{-1} and 17.1 km s^{-1} at 20 parsecs. Of the three surveys, the last has received least attention. While Weis (1986, 1987, 1988) has obtained (B)VRI photometry for many of the brighter ($m_r \leq 13.5$) red stars in the NLTT, it is only recently that systematic attempts have been made to identify nearby stars amongst the fainter members of that catalogue (Reid & Cruz, 2001; Salim & Gould, 2002) Thus, there is a clear potential for bias against stars with low tangential motions in both the pCNS3 and the VC^2 sample.

We can test for kinematic bias by comparing the proper motions and transverse motions of the full VC^2 sample against similar data for the subset of stars which are included in the objective prism surveys (Vyssotsky, 1956; Upgren *et al.*, 1972). Since the latter stars were identified based on spectral type, that sample should be free of any kinematic selection effects. Two hundred and nine of the 448 systems in the VC^2 sample are in the Vyssotsky catalogue, while the Upgren *et al.* survey contributes four systems.

Most of the spectroscopically-selected stars are early-type M dwarfs, and those stars lie predominantly at larger distances in the VC^2 sample. This is illustrated in the upper panels of Figure 4. Since the average distance of the spectroscopic subset is higher than the full sample, we must compare the tangential velocity distributions, rather than the proper motion distributions. That comparison is shown in the lower panels of Figure 4, where the dotted line in the right-hand panel marks the fractional contribution of the spectroscopic subset to the full sample. If there were a significant bias against stars with low transverse motions, we would expect the proportion of spectroscopically-selected stars to rise with decreasing V_{tan}. The data show little evidence for that effect. Dividing the distribution into two subsets, with $V_{tan} \leq 20$ kms^{-1} and $V_{tan} > 20$ kms^{-1}, the ratios $\frac{N_{prism}}{N_{tot}}$ are $44.0 \pm 7.4\%$ and $48.6 \pm 4.7\%$, respectively.

Our tests therefore reveal no evidence for significant bias in the VC^2 sample either against stars lying within 10 degrees of the Galactic Plane, or against stars with low tangential motions. On that basis, we conclude that the VC^2 sample provides a reliable dataset for examining the space density and kinematics of the local Galactic Disk population.

3. The Luminosity Function

3.1. The Luminosity Function

We next consider how the revised distances obtained by Hipparcos affect the nearby-star luminosity function, $\Phi(M_V)$. We also take this opportunity to redetermine $\Phi(M_V)$ for earlier-type (BAFGK) main-sequence stars in the Solar Neighbourhood, and to identify lower-mass

companions to those stars which should be added to the PMSU M dwarf statistics. Despite the availability of Hipparcos data for more than half a decade, many recent luminosity-function analyses are still based on the statistics compiled by Wielen, Jahreiß & Krüger (1983) from the second Catalogue of Nearby Stars (Gliese, 1969; CNS2) and its supplement (Gliese & Jahreiß, 1979). An exception is the sample discussed by Kroupa, 2001. Clearly, the systematics evident in Figure 1 have a significant influence on our estimate of the local density of main-sequence stars.

The Hipparcos catalogue has a formal completeness limit of

$$V \; = \; 7.9 \; + \; 1.1 sin|b|$$

so the 25-parsec sample is effectively complete over the whole sky for $M_V \leq 5.9$. However, since the mission involved pointed observations of pre-selected targets, the survey includes a high proportion of stars known or suspected of being in the immediate Solar Neighbourhood. Indeed, Jahreiß and Wielen (1997) argue that the Hipparcos catalogue is essentially complete to $M_V = 8.5$ for stars within 25 parsecs of the Sun, providing a useful complement to the $8 < M_V < 16$ VC[2] sample.

We have identified 831 Hipparcos stars with $\pi_H \geq 40$ milliarcseconds (mas) and $M_V \leq 8.0$. Three issues need to be addressed before deriving a luminosity function from this dataset: the evolutionary status of the individual stars; binarity and multiplicity; and the local intermix of stellar populations. The first and last considerations are illustrated in Figure 5, which plots the (M_V, (B-V)) colour-magnitude diagram for all 1477 stars in the Hipparcos catalogue with $\pi_H \geq 40$ mas. Evolved stars clearly make a significant contribution at brighter magnitudes, and we have excluded them by eliminating stars which meet the following criteria,

$$M_V \; < \; 7.14(B-V) - 1.0, \text{ and } M_V \; < \; 5.0$$

This removes 41 stars from the sample.

Figure 5 includes a number of stars lying well below the disk main sequence. Most are fainter than M_V=8.0 and are either white dwarfs, stars with substantial uncertainties in the measured parallax, or stars lacking (B-V) colours. Four stars, however, lie just below the main sequence with $6 < M_V < 8$. These are the halo subdwarfs HIP 18915 (HD 25329, [Fe/H]=-1.6), HIP 57939 (HD 103095, [Fe/H]=-1.4), HIP 67655 (HD 120559, [Fe/H]=-0.94) and HIP 79537 (HD 145417, [Fe/H]=-1.25). While the statistics are not overwhelming, a total of four subdwarfs in a sample of ~ 650 FGK disk dwarfs implies a local number ratio of $\sim 0.6 \pm 0.3\%$, a factor of three higher than the density normalisation adopted for the halo in most Galactic structure analyses. All four stars are excluded from the present analysis.

Finally, we have checked SIMBAD for references to binary and multiple systems amongst

the remaining 786 stars. Thirteen systems have wide companions listed separately in the Hipparcos database, while a further 213 have unresolved companions at small separations or wide companions which are not included in the Hipparcos dataset. Where necessary, we have adjusted the photometry to allow for the contribution from fainter components, most notably in the case of HIP 66212 (HD 110836), which the uncorrected Hipparcos data place well above the main sequence. As illustrated in Figure 6, these corrections move a handful of primary stars to magnitudes fainter than M_V=8.0.

Even after applying photometric adjustments, a small number of stars still lie well above the main sequence in figure 6. Some (e.g. Gl 610) may be unrecognised binaries. Several, however, are primaries in binary systems (e.g. Gl 795A, GJ 1161A, Gl 118.2A), and the presence of the known secondary may affect either the photometry or the astrometry. Others are metal-rich stars (e.g. Gl 614, Gl 848.4 and HD 217107, all known to harbour extrasolar planets), while still others, lying near the base of the subgiant branch, may be slightly evolved (e.g. Gl 19, Gl 368). Further spectroscopy and photometry are required to resolve these issues completely.

We noted above that the Hipparcos dataset is expected to be effectively complete within 25 parsecs for stars with $M_V < 8.5$. We can test this hypothesis using the same techniques applied to the PMSU M dwarfs in §2. Figure 7 plots the run of density with distance for systems where the primary has $M_V = 4.5 \pm 0.5.5.5 \pm 0.5, 6.5 \pm 0.5$, and 7.5 ± 0.5. The first point marks the average density within a sphere, radius 16 parsecs, centred on the Sun; subsequent point plot the densities within annuli of radii 16 to 18, 18 to 20, 20 to 22 and 22 to 25 parsecs. Given Poisson uncertainties, there is no evidence for a significant decline in completeness as one approaches the 25-parsec distance limit.

Our final sample includes 764 Hipparcos systems with $d < 25$ parsecs and $M_V < 8.0$. A further twelve binaries have primaries with $8 < M_V < 9$. Four of those stars are already included in the PMSU sample, while three stars lie beyond 22 parsecs (the PMSU distance limit appropriate to this absolute magnitude). The remaining five stars are added to the PMSU sample. We also extend coverage to $M_V \geq 16$ by adding data for the three systems currently known with $d < 5$ parsecs and $\delta > -30^o$ (GJ 1111, Gl 406 and LHS 292). Table 4 gives final statistics for the combined PMSU and Hipparcos 25-parsec samples, and Figure 8 plots the composite luminosity function, $\Phi(M_V)$.

We have compared our results against the luminosity function derived by Wielen, Jahreiß & Krüger (1983). The space densities derived here are systematically lower than in the earlier study, reflecting the systematic errors present in pre-Hipparcos distance estimates. Kroupa (2001) finds similar results in his analysis. Overall, we derive a local number density of 0.106 main sequence stars pc^{-3}, and a density of 0.0725 systems pc^{-3}. With evolved systems

contributing a further 41 systems within 25 parsecs (6.3×10^{-4} pc^{-3}), the average separation between systems is ~ 2.4 parsecs.

3.2. Binarity and Multiplicity

The 764 systems in our Hipparcos 25-parsec upper main-sequence sample include 538 single stars, 204 binaries (including 8 low amplitude spectroscopic binaries from Nidever *et al.*, 2002), 22 triples and 4 quadruple systems. The resultant multiplicity fraction is only $30.1 \pm 2.4\%$, somewhat lower than the value of 44% derived in the standard reference for this subject, Duquennoy & Mayor's (1991, DM91) analysis of observations of solar-type dwarfs. This discrepancy may reflect poorer observational coverage of the Hipparcos sample. Even with the addition of the extensive radial velocity data from the Lick/Keck planet-search survey, summarised by Nidever *et al.* (2002), 98 stars lack radial velocity measurements, and we noted in the previous section that a number of stars lie above the main sequence, suggesting unrecognised binarity.

An alternative possibility is that the multiplicity fraction measured for the 25-parsec sample is more reliable than the DM91 statistics. The lower binarity might be a consequence of the larger magnitude range spanned by the present sample, since M dwarfs are known to have a lower fraction of stellar companions than solar-type stars (Fischer & Marcy, 1992; RG97). In addition, the improved parallax data lead to a better-defined sampling volume for the present dataset than for the DM91 dataset. We explore these issues here.

In analysing the multiplicity of solar-type stars, Duquennoy & Mayor's intention was to define a volume-limited sample, including systems with spectral types between F7 and G9, declinations $\delta > -15$ deg and parallaxes exceeding 45 milliarcseconds. However, since the parallaxes were drawn from the CNS2, they are subject to the systematic errors and potential biases illustrated in Figure 1. Fortunately, all of the DM91 stars are included in the Hipparcos catalogue.

Figure 9 compares parallax data listed in the CNS2 against Hipparcos measurements for the DM91 reference sample. As expected, over 40% of the sample lie beyond the nominal 25-parsec distance limit, including almost all stars with (B-V)>0.8, most of which are subgiants. Only 102 systems have $\pi_H \geq 45$ milliarcseconds. However, of those 102 systems, 42 are double or multiple, giving a multiplicity fraction of 41±7%, consistent with the value of 44% derived for the full dataset in DM91. Observational bias in the DM91 sample is therefore not likely to be responsible for the discrepancy with respect to the Hipparcos 25-parsec sample.

Even with the extensive temporal coverage and high accuracy provided by the CORAVEL

radial velocity observations, it is likely that a significant number of binary systems remain unrecognised amongst the DM91 G-dwarf sample. Binary systems with high inclination and/or long period have low velocity amplitudes, and are therefore more difficult to detect. Duquennoy & Mayor concluded that their analysis might underestimate the binary fraction amongst G dwarfs by approximately one-third, implying a true multiplicity close to 60%. On the other hand, 47 of the 60 "single" stars in the $\pi_H \geq 45$ mas DM91 sub-sample are included in the Lick/Keck planet search program: 46 are classed as having stable radial velocities ($\sigma_V < 0.1$ kms^{-1}); only HIP 98819 (Gl 779) is identified as a confirmed spectroscopic binary (Nidever *et al.*, 2002).

Based on these results, we take 60% as a likely upper limit for the multiplicity of the upper main-sequence stars in the Hipparcos 25-parsec sample. Given the relatively sparse observational scrutiny, we assume that the known secondaries are characteristic of the sample as a whole, and therefore allow for potential "missing" binary companions by giving double weight to known binary components in the statistical analysis. Figure 10 shows the resultant effect on $\Phi(M_V)$: the space densities are still systematically lower than the Wielen *et al.* (1983) values. The overall space density becomes 0.112 stars pc^{-3}.

4. The Mass Function

4.1. The Mass-Luminosity Relation

The mass-luminosity relation is a key ingredient in transforming the stellar luminosity function to a mass function. Since we have only B, V data for most of the stars in the present sample, we require a relation between mass and M_V. In general, masses can be derived only for stars in binary systems (gravitational lensing offers the potential for deriving accurate masses for single stars, but requires particular source-lens geometries). Henry & McCarthy (1993) provided the first extensive analysis of lower main-sequence astrometric binaries. They derive a three-segment fit in the (M_V, log(mass)) plane, extending from $2M_\odot$ to the hydrogen-burning limit. Together with their mass-M_K and mass-M_{bol} relations, this calibration has served as the primary reference over the last decade.

Most recent attention has centred on low-mass stars, with the addition of new data from high-precision HST (Henry *et al.*, 1999) and ground-based astrometry, and from high-accuracy radial velocity measurements (Delfosse *et al.*, 1999; Ségransan *et al.*, 2000). Delfosse *et al.* (2000: D00) have used these new observations to derive a revised mass-M_V relation for lower main-sequence stars,

$$\log M \;=\; 10^{-3} \times [0.3 + 1.87 M_V + 7.614 M_v^2 - 1.698 M_V^3 + 0.06096 M_v^4]$$

As Figure 11 shows, this relation predicts higher masses by 10 to 15% than Henry *et al.'s* calibration for $11 < M_V < 15$.

Delfosse *et al.* limit their analysis to M dwarfs, and Henry *et al's* piecewise mass-M_V relation extends only to $2M_\odot$, but the Hipparcos 25-parsec sample includes more massive A- and B-type stars. We have therefore used the data compiled by Andersen (1991) for eclipsing binary systems to derive an empirical mass-M_V relation covering the upper main-sequence. That relation is

$$\log M \;=\; 0.477 - 0.135 M_v + 1.228 \times 10^{-2} M_v^2 - 6.734 \times 10^{-4} M_V^3$$

and is plotted in Figure 11. We combine that relation with the D00 result, setting the boundary between the two calibration at M_V=10.0, where the agreement is better than 5%.

In addition to these empirical calibrations, Kroupa, Tout & Gilmore (1993, KTG) derived a semi-empirical mass-M_V relation. Adopting the Wielen *et al.* (1983) luminosity function as a reference, they represent the mass function as a three-component power-law, and vary the indices to minimise residuals in the mass-M_V relation. Figure 11 compares their derived relation against the empirical results. The KTG calibration, spanning absolute magnitudes between M_V=+2 and +17, matches the D00 relation at low masses, and lies up to 8% below the empirical relation (i.e. predicts lower masses at a given M_V) for solar-mass stars.

4.2. The Present-day Mass Function

We have computed present-day mass functions using both the D00 empirical calibration and the KTG semi-empirical relation, extending both to higher masses using our fit to the Andersen eclipsing binary dataset. Figure 12 shows the results derived from the empirical calibration. Defining

$$\xi(M) \;=\; \frac{dN}{d\log M} \text{ and } \psi(M) \;=\; \frac{dN}{dM}$$

the uppermost panel plots $\xi(M)$ for the Hipparcos 25-parsec and the PMSU samples (i.e. the dataset used to construct $\Phi(M_V)$ in Figure 8). The dotted histogram shows the mass function derived from single stars and primaries in multiple systems. The middle panel in Figure 12 plots $\xi_{2B}(M)$, where double weight is given to the Hipparcos 25-parsec secondary components (i.e. the dataset used to construct Figure 10). Adding the hypothetical as-yet-undiscovered binaries produces little change in the overall morphology. Integrating the mass functions, we derive a local mass density of $\rho_{MS} = 0.0310 M_\odot pc^{-3}$ from $\xi(M)$ and 0.0338 $M_\odot pc^{-3}$ when double weight is given to the secondaries in the Hipparcos sample. We note that white dwarfs contribute a further 0.004 $M_\odot pc^{-3}$ (RG97).

We have also used the empirical mass-M_V relation to re-compute the mass function derived from the northern ($\delta \geq -30\,\mathrm{deg}$) 8-parsec sample. The original sample from RG97 has been updated to take into account Hipparcos parallax data and new stellar companions (Reid *et al.*, 1999; R99). Chabrier & Baraffe (2000) and Kroupa (2001) have suggested that this sample provides unreliable statistics, both through the inclusion of stars whose distances rest on photometric/spectroscopic parallax estimators, and through incompleteness. Neither objection is valid. As emphasised in R99, 100 of the 104 systems have accurate ($\epsilon < 10\%$) trigonometric parallax measurements, while only a handful of addition have been identified since 1997. The most recent is 2MASS J1835379+325954, an M8 dwarf at 5.7 parsecs (Reid *et al.*, 2002a). As discussed in that paper, the >30% deficit in number density between the 8-parsec and extrapolated 5-parsec sample (Henry *et al.*, 1997) includes a substantial contribution from bright ($M_V < 14$) stars, and probably overestimates the shortfall by at least a factor of two.

The mass function derived from the 8-parsec sample is plotted in the lowermost panel of Figure 12. Again, the single star/primary mass function is plotted as a dotted histogram. Below 1 $M_\odot$, the results are statistically identical to those based on the composite Hipparcos 25-pc./PMSU analysis (i.e., employing a 5-parsec limit at $M_V > 15$). The total mass density derived by integrating $\xi_8(M)$ is 0.0288 $M_\odot pc^{-3}$, the lower value reflecting the relative scarcity of G dwarfs within 8 parsecs of the Sun[4].

Following Salpeter (1955), it is convenient to represent the mass function as a power-law,

$$\xi(M) \;=\; M^{-\alpha+1} \text{ and } \psi(M) \;=\; M^{-\alpha},$$

where $\alpha = 2.35$ is the Salpeter slope. The mass functions plotted in Figure 12 are all well represented by a two-component power-law. Both Hipparcos/PMSU analyses are consistent with $\alpha = 1.35 \pm 0.2$ for $0.1 < \frac{M}{M_\odot} < 1$ and $\alpha = 5.2 \pm 0.4$ for $M > 1 M_\odot$. The steep slope at masses above $1 M_\odot$ emphasises the fact that $\xi(M)$ is the present-day mass function (Miller & Scalo, 1979); our calculations take no account of higher mass stars which have evolved off the main sequence over the lifetime of the Galactic disk. The 8-parsec sample has fewer high mass stars than the Hipparcos dataset, but still shows a clear break near $1 M_\odot$, and we derive $\alpha = 1.15 \pm 0.2$ for $0.1 < \frac{M}{M_\odot} < 1$, matching the original RG97 analysis. In each case, fitting to the single-star/primary dataset flattens the distribution below $1 M_\odot$, giving $\alpha \sim 1$, since secondaries make a proportionately higher contribution at lower masses.

[4]We note that the 2σ deficit of G dwarfs in a comparison of the 8-parsec and 25-parsec samples has the same statistical weight as the 2σ excess of M_V=16 stars in a comparison between the 5-parsec and 8-parsec samples. There appears to be little concern, however, over 'missing' G dwarfs within 8 parsecs of the Sun.

Figure 13 compares results from the empirical and semi-empirical mass-M_V calibrations. The derived mass functions are in broad agreement, particularly at low masses. As might be expected from Figure 11, the main differences arise at near-solar masses. Rather than a single break at $\sim 1 M_\odot$, the semi-empirical relation produces changes in slope at $\sim 0.7 M_\odot$ and $\sim 1.1 M_\odot$ (masses close to the break points chosen by KTG in their calibration procedure).

Fitting $\xi_{KTG}(M)$ as a combination of power-laws, we find $\alpha = 1.3 \pm 0.15$ for $0.1 < \frac{M}{M_\odot} < 0.7$ (fitting $0.15 < \frac{M}{M_\odot} < 0.7$ gives $\alpha = 1.03 \pm 0.11$), $\alpha = 2.8 \pm 0.4$ for $0.7 < \frac{M}{M_\odot} < 1.1 M_\odot$, and $\alpha = 4.8 \pm 0.15$ for $M > 1.1 M_\odot$. Not unexpectedly, these results are very similar to those derived by Kroupa (2001). Integrating over the mass function, we find that main sequence stars contribute 0.0300 $M_\odot pc^{-3}$ to the local mass density. As with the empirical calibration, allowing for additional binaries amongst the Hipparcos 25-parsec sample increase ρ_{MS} by $\sim 10\%$.

Comparing $\xi(M)$ and $\xi_{KTG}(M)$, the main difference is the steepening of the latter between ~ 0.7 and 1.0 $M_\odot$, reflecting the differences in the mass-M_V relations evident in Figure 11. Additional calibrating binaries in this mass range would be clearly be very useful. That discrepancy apart, there is considerable similarity between the global properties of the two present-day mass functions plotted in Figure 13: $\alpha \sim 1.2$ at low masses; $\alpha \sim 5$ at super-solar masses; and, depending on the binary fraction, an integrated mass density of 0.030 to 0.034 $M_\odot pc^{-3}$.

4.3. The Initial Mass Function

The mass function, $\xi(M)/\psi(M)$, specifies the relative number of main sequence stars as a function of mass in the local Galactic disk at the present time. A more fundamental quantity is the initial mass function, denoted here as $\Xi(M)$ (logarithmic mass units) or $\Psi(M)$, the relative number of stars forming as a function of mass. Three factors need to be taken into account in converting the present-day mass function to the initial mass function: stellar evolution; the density distribution perpendicular to the Plane; and the local mix of stellar populations.

Salpeter (1955) originally pointed out the necessity of allowing for evolution beyond the main sequence in computations of the 'original mass function'. M dwarfs have main sequence lifetimes, τ_{MS}, well in excess of 20 Gyrs, so $\xi(M)$ includes low-mass stars spanning the full history of star formation in the Disk. Higher mass stars have shorter hydrogen-burning lifetimes, and $\xi(M)$ only takes account of stars with ages, $\tau < \tau_{MS}$. Thus, the present-day census includes only a fraction of the total population if τ_{MS} is less than the age

of the Galactic disk, τ_{disk}. Correcting the observed numbers for this effect requires that we estimate the age of the disk and adopt a stellar birthrate as a function of time.

Binney, Dehnen & Bertelli (2000) summarise the various techniques which have been used to estimate the age of the local disk population. Those include analyses of the low-luminosity cutoff in the disk white dwarf luminosity function, measurements of isotopic ratios, isochrone matching for individual stars and quantitative analysis of the distribution of stars in the HR diagram. Individual age estimates range from 7 to 15 Gyrs; we adopt $\tau_{disk} = 10$ Gyrs in the present calculations. Following the discussion in PMSU3, we assume a constant star formation rate, so the correction factor is given by

$$f_{MS} \; = \; \frac{\tau_{Disk}}{\tau_{ms}}, \text{for } \tau_{MS} < \tau_{Disk}$$

These corrections are applied on a star-by-star basis to the Hipparcos sample, with the appropriate main-sequence lifetimes computed from

$$\log \tau_{MS} \; = \; 1.015 \; - \; 3.491 \log M \; + \; 0.8157 (\log M)^2$$

This relation is derived from the solar abundance models computed by Schaller *et al.* (1992).

The decrease in main-sequence lifetime with increasing mass also requires accounting for the vertical density distribution, $\rho(z)$. Velocity dispersion increases with age, so the younger average age of higher-mass stars leads to lower velocities and a density distribution which is confined more closely to the Plane. Thus, a local volume-limited sample of the latter stars, drawn from near the galactic mid-Plane, includes a larger fraction of the total population.

We correct for this effect following Miller & Scalo. The vertical density distribution of disk stars can be represented by an exponential distribution, scaleheight z_0. Most recent studies derive a value of $z_0 \sim 250$ parsecs for long-lived main-sequence stars ($M_V > 4$); younger upper main-sequence stars, $M_V < 3$, have lower velocity dispersions and a steeper density distribution, $z_0 \sim 100$ parsecs (Haywood *et al.*, 1997; Siegel *et al.*, 2002). We adopt a scaleheight of 170 parsecs for stars with intermediate absolute magnitudes, $3 < M_V < 4$. Deriving accurate estimates of surface density from $\psi(M)$ is a complex operation, requiring modelling of the overall potential (see, for example, Kuijken & Gilmore, 1989). We assume that the effective surface densities, Σ, scale linearly with z_0, i.e.

$$\Sigma \; \propto \; \rho_0 z_0$$

where ρ_0 are the volume densities plotted in Figures 12 and 13.

Finally, since we aim to derive $\Xi(M))$ for the disk, we need to take account of Solar Neighbourhood stars which are members of other stellar populations. For present purposes,

we consider three components: disk, thick disk and halo (stellar, not dark matter). While last component makes a negligible contribution locally (§3.1), approximately 10% of the stars in the immediate Solar Neighbourhood are part of the more extended thick disk (see §5.2). The full characteristics of the latter population, particularly the abundance and age distribution, remain uncertain, but starcounts at $z > 1000$ pc. demonstrate there are few. if any, stars younger than a few Gyrs, and that the vertical density distribution has a scaleheight three to four times that of $M_V > 4$ disk stars (Siegel *et al.*, 2002). Given those results, we assume that 90% of local stars with $M_V \geq 4$ are disk dwarfs, and scale $\psi(M)$ accordingly.

Figure 14 shows the initial mass functions derived from $\xi(M)$ and $\xi_{KTG}(M)$; both datasets are based on the observed Hipparcos 25-parsec and PMSU samples (i.e., we have not applied corrections for potential undetected secondary components). In both cases, $\Xi(M)$ can be represented as a two-component power-law: with the empirical mass-M_V relation, the data are consistent with $\alpha = 1.3 \pm 0.2$ at $M < 1.1 M_\odot$, and $\alpha = 2.8 \pm 0.25$ at higher masses; adopting the semi-empirical mass-M_V relation gives $\alpha = 1.1 \pm 0.15$ at $M < 0.6 M_\odot$, and $\alpha = 2.5 \pm 0.15$ at higher masses, consistent with results derived by Kroupa (2001). Reducing the assumed age of the Disk to 8 Gyrs steepens α at high masses by ~ 0.15; increasing τ_{disk} to 12 Gyrs flattens α to a similar extent.

4.4. Modelling $\Xi(M)$: power-laws or log-normal functions?

Power laws provide a mathematically simple means of representing the stellar initial mass function, and give an adequate match to the data plotted in figure 14. Some recent studies, however, find that mass functions of this form are less successful in matching data for young clusters and associations. In particular, Hillenbrand & Carpenter (2000) find that $\psi(M)$ peaks at $\sim 0.15 M_\odot$ in the central regions of the Orion Nebula Cluster[5]. Miller & Scalo (1979) provided an alternative to power laws in their log-normal representation of the initial mass function,

$$\Xi(M) \; = \; C_0 \, \exp(-C_1 (\log M - C_2)^2)$$

where C_0, C_1 and C_2 are constants, defining the normalisation, width and maximum of the initial mass function.

The main impact of adopting a log-normal representation of $\Xi(M)$ is twofold: first, the existence of a preferred mass (10^{C_2}) has implications for star formation models; second,

[5]We note that Luhman *et al.*(2000), using a different set of evolutionary tracks, find that the ONC mass function is consistent with a power-law, $\alpha \sim 1$, to $\sim 0.04 M_\odot$.

the extrapolation below the hydrogen-burning limit affects expectations of the frequency of brown dwarfs. Neither of the IMFs plotted in Figure 14 extends to substellar masses. Measuring $\Psi(M)$ at those masses in the field is complicated severely by the rapid luminosity evolution of brown dwarfs, as discussed by R99. Modelling the mass function as a power law, R99 found that a simple extension of the low-mass star IMF ($\alpha = 1.3 \pm 0.3$) provides a reasonable match to the (still scarce) observations. Chabrier (2002) arrives at similar conclusions. However, the field brown dwarf sample is likely to be dominated by longer-lived, higher-mass objects, $M > 0.04 M_{\odot}$. As figure 14 shows, within those limits (0.04 to $0.08 M_{\odot}$), there is relatively little difference in slope between the Miller-Scalo functions and an $\alpha \sim 1$ power law. More extensive observations of young clusters, and improved models for pre-main sequence dwarfs, still offer the best prospects of establishing $\Psi(M)$ at these low masses.

We have matched log-normal distributions against the observations. We have fixed $C_2 = -0.9$ and defined a goodness of fit statistic,

$$\chi^2_{\nu} \; = \; \Sigma(\frac{(O-C)^2}{\epsilon^2})/\nu$$

where O, C are the observed and predicted values of $\Xi(M)$, ϵ is the associated Poisson uncertainty, and $\nu = n_{bin} - 2$. We allow both C_0 and C_1 to vary. The best-fit results are C_1=1.0 for $\Xi(M)$ and C_1=1.2 for $\Xi_{KTG}(M)$ (the values of C_0 have no physical significance, since our density scaling has an arbitrary zeropoint). These results are plotted in figure 14, together with the best-fit match for C_1=1.15, the original value derived by Miller & Scalo (1979). The χ^2_{ν} values for those fits are 8.34 and 6.08, respectively (for $\nu = n_{bin} - 3$) ; in comparison, the power-law representation gives $\chi^2_{\nu} = 4.34$ and 4.66, respectively.

In summary, log-normal Miller-Scalo functions provide a poorer representation of the overall shape of the derived IMFs than simple power-law fits. Having noted that, one should bear in mind the caveat that the differences between the two 'observed' functions plotted in Figure 14 highlight the continued potential for systematic effects introduced by changes in the mass-luminosity relation. Nonetheless, the main challenge facing star formation theory appears to lie in providing an explanation for the change in power-law index between 0.7 and 1.1 $M_{\odot}$.

5. Galactic Disk Kinematics

In PMSU1 we used our observations of the VC sample to study the motions of local stars, and in PMSU2 we examined the different kinematics exhibited by M dwarfs with and without detectable Hα emission. Those analyses were based on radial velocities derived from

the intermediate resolution spectra used to measure bandstrengths and determine spectral types. We can re-examine those issues using the more accurate distances and radial velocities measured for the VC^2 sample.

5.1. Solar Motion and the Schwarschild velocity ellipsoids

We have used standard techniques (Murray, 1983) to parameterise the kinematics of the M dwarfs in the VC^2 sample. We calculate the Solar Motion and Schwarzschild ellipsoid parameters for (U, V, W) Galactic co-ordinates, where U is positive towards the Galactic Centre, V positive in the direction of rotation, and W positive towards the North Galactic Pole. This matches the co-ordinate system used in the pCNS3.

This standard calculation measures the velocity distributions of stars within a small spherical volume, centred on the Sun and lying near the midpoint of the Galactic Plane. Wielen (1974, 1977) has argued that weighting the velocity dispersion by the W velocity (effectively, the inverse residence time in the Plane) provides a more useful estimator. Those dispersions are calculated as follows:

$$\sigma_U^2 = \sum_i (|W_i| U_i^2) / \sum_i |W_i|$$

$$\sigma_V^2 = \sum_i (|W_i| V_i^2) / \sum_i |W_i|$$

$$\sigma_W^2 = \frac{1}{2} \sum_i (|W_i| W_i^2) / \sum_i |W_i|$$

Both sets of velocity dispersions are listed in Table 5, together with the mean velocity relative to the Sun, the Solar Motion. The results are consistent both with our previous studies, based on lower-accuracy radial velocities, and with other analyses of nearby star samples (e.g. Dehnen & Binney, 1998).

As in PMSU2, we have segregated M dwarfs in the VC^2 sample with measureable Hα emission. In the PMSU2 analysis, the low-resolution spectroscopy limited this sample to stars with equivalent widths exceeding 1.0Å; in the present sample, with the higher-resolution PMSU3 echelle data, the effective limit is 0.1Å. Eighty-three stars in the VC^2 sample meet this criterion, and the resulting mean kinematics are listed in Table 5. As discussed in PMSU2, Hα emission declined with increasing age, so it is no surprise that the unweighted velocity dispersions are significantly lower than those of the full VC^2 sample. In contrast, the weighted velocity dispersions are markedly higher. This reflects the influence of a small number of stars with large W velocities (e.g. GJ 1054, W=-95.3 km s^{-1} and Gl 630.1, or CM

Dra, W=-83 km s^{-1}), and illustrates the vulnerability of this calculation to small number statistics.

We have also determined the mean kinematics for stars in the Hipparcos 25-parsec sample. As noted above, 98 of the 764 systems in this sample lack radial velocities, and those stars are not included in our statistics. Most of the latter systems have low proper motions, as one might expect given their pre-Hipparcos obscurity - seventy-four (∼75%) have $\mu < 0.3''$ yr^{-1} and 73 have $V_{tan} < 30$ km s^{-1} . Ignoring those stars in the present analysis may affect the derived (U, V, W) distributions at low velocities, although the comparisons in the following section suggest that this is not a severe effect.

We have divided the Hipparcos dataset into two sub-samples: 138 systems with $M_V < 4$ (137 with V_r measurements); and 626 systems $M_V \geq 4$ (528 with radial velocities). Table 5 lists the mean kinematics those datasets, and Figure 15 compares the (V, U) and (W, U) velocity distributions against data for the VC^2 sample. The fainter Hipparcos stars are kinematically indistinguishable from the M dwarf sample, as one would expect, given that both datasets should sample the same underlying population - disk dwarfs with ages spanning the star formation history of the Galactic disk. The brighter Hipparcos stars have significantly lower velocity dispersions than even the dMe sample, reflecting the short main-sequence lifetimes and younger ages of these more luminous stars. The derived kinematics for those stars are consistent with recent studies.

5.2. The M-dwarf velocity distribution and the thick disk

The r.m.s. velocity dispersions derived in the previous section provide a simple one-parameter characterisation of the velocity distribution in each component. While useful as a simple means of comparing difference stellar samples, that parameterisation can be misleading if the underlying velocity distribution is non-Gaussian in nature. Probability plots (Lutz & Upgren, 1980) provide a method of examining the velocity distributions in more detail: if a given sample is drawn from a Gaussian distribution, plotting the cumulative distribution in units of the measured r.m.s. dispersion gives a straight line.

Figure 16 shows (U, V, W) probability plots for the full VC^2 sample, the dMe stars from that sample, and both subsets of the Hipparcos dataset ($M_V > 4/M_V < 4$). The full VC^2 dataset and the fainter Hipparcos sample have very similar velocity distributions, suggesting that even though the latter sample is not complete, the subset of stars with measured radial velocities is unbiased. The brighter Hipparcos stars and the dMe dwarfs, samples dominated by younger stars, have velocity distributions closest to those expected for

Gaussian dispersions, although both, particularly the emission-line stars, become non-linear at extreme velocities. A number of the higher-velocity dMe dwarfs are known to be close binaries (e.g. CM Dra). These stars could be older systems, where tidal locking maintains enhanced rotational velocities and stronger Hα emission.

All four datasets exhibit near-linear distributions at low velocities, suggesting that each includes a core subset of stars with Gaussian velocity distributions. We have measured the slope of the central regions for each distribution. In U and W, the gradients are derived for the range $-1 < \sigma < 1$; the V distributions become non-linear more rapidly at negative velocities (lagging the Solar rotational velocity), and we fit the slope in the range $-0.5 < \sigma < 2$. The resulting measurements are listed in Table 5.

We propose that the linear core in these probability distributions represents the disk population in each sample. The two younger datasets, the brighter Hipparcos stars and the dMe dwarfs, have been subjected to less secular scattering, and therefore have lower velocity dispersions. The non-linearities are more pronounced at large $|\sigma|$ in the other two samples and, in at least U and W, are symmetric, suggesting the presence of a second, higher velocity dispersion component. The obvious candidate for the latter is the thick disk. Identified originally by Gilmore & Reid (1983), the thick disk is evident as a flattening of the density law, $\rho(z)$, at $\sim 1 - 1.5$ kpc. above the Plane. Initial analyses of $\rho(z)$ suggested a low local density normalisation ($\rho_{TD}(z = 0) \sim 0.02\rho_{disk}(z = 0)$) and high scaleheight (>1.3 kpc), but more recent studies (Haywood et al, 1997; Siegel et al, 2002) favour a higher normalisation ($\sim 5\%$) and a smaller scaleheight (0.7 to 1 kpc.). Its origin remains uncertain, but, as noted in the previous section, the scarcity of main-sequence A and F stars indicates $\tau > 3$ Gyrs. There are no direct, unbiased measurements of the abundance distribution.

The rotational properties of the thick disk are not yet well established, complicating analysis of the V-velocity distributions. However, we do not expect a significant Solar Motion in either U or W, while a stellar component with a larger scaleheight must also have a higher σ_W than disk dwarfs. Modelling the latter velocity distributions should therefore provide insight into both thick disk kinematics and the local density normalisation.

We have matched the observed W-velocity probability distributions of the VC^2 and faint Hipparcos samples against models derived by combining two Gaussian components (σ_1, σ_2), with a relative normalisation, $f = \frac{N_1}{N_2}$. We set $\sigma_1 = 16$km s^{-1} , matching the core of the observed distribution, and define the mean velocity as W=-8 km s^{-1} (VC^2) and -6 km s^{-1} (Hipparcos). We let σ_2 vary from 18 km s^{-1} to 60 km s^{-1} in steps of 2 km s^{-1} , varying f between 0.02 and 0.20 at each velocity. At each step, we compute the rms residuals

$$R_s \; = \; \Sigma(W_i - W_c)^2$$

where W_i is the observed velocity and W_C the predicted velocity for the measured σ_i (the abscissa in the probability plots). R_s is computed for the range $-2.5 < \sigma_i < 2.5$ to minimise the effect of outliers in the observed velocity distribution.

Matched against the models, both datasets exhibit a broad minimum in R_s centred at $\sigma_2 \sim 36$km s^{-1} , $f \sim 0.12$. There is reasonable agreement between the model and the data for $34 < \sigma_2 < 48$ km s^{-1} and $0.1 < f < 0.2$ for the VC^2 sample, and for $34 < \sigma_2 < 42$ km s^{-1} and $0.1 < f < 0.16$ for the Hipparcos dataset. In general, σ_2 and f are anti-correlated in those solutions. Figure 17 illustrates several examples. None of the models provide a good match to the data at $|\sigma| > 2.5$, where small number statistics can affect the observed distribution.

Analysing the U-velocity distribution gives similar results. Setting $\sigma_1 = 34$ km s^{-1} , and matching the distribution for $|\sigma| < 2.5$, the best-fit values are $\sigma_2 = 60$ to 64 km s^{-1} , $f = 0.1$ to 0.12 for the VC^2 sample, and $\sigma_2 = 64$ to 70 km s^{-1} , $f = 0.1$ to 0.14 for the Hipparcos dataset. Both datasets are consistent with approximately 10% of Solar Neighbourhood stars being members of the higher-velocity component.

Summarising these results, a two-component Gaussian distribution with velocity dispersions ($\sigma_1 = 16$km s^{-1} , $\sigma_2 \sim 36$km s^{-1} , $f = 0.12$) provides a good representation of the observed W-velocity distribution of Solar neighbourhood disk dwarfs. A two-component Gaussian with ($\sigma_1 = 34$km s^{-1} , $\sigma_2 \sim 62$km s^{-1} , $f = 0.12$) matches the observations in U. In both U and W, approximately 10% of the sample resides in the higher velocity-dispersion component. Given the results from recent starcount analyses, it seems reasonable to identify the latter stars as the local constituents of the thick disk.

5.3. Ultracool M dwarfs and the thick disk

Reid *et al.* (2002b) have recently presented high-resolution echelle observations of a photometrically selected sample of ultracool M dwarfs (spectral types later than M7). One of the surprising results from that study concerns the velocity distributions, which have more similarity to our analysis of dMe dwarfs than the kinematics of the full VC^2 sample. This is unexpected, since almost all ultracool M dwarfs are expected to be hydrogen-burning stars, albeit with masses very close to the hydrogen-burning limit. With main-sequence lifetimes exceeding 10^{12} years, ultracool dwarfs, like earlier-type M dwarfs, should span the full age range of the Galactic Disk. One would expect such stars to have experienced a similar history of dynamical interactions, leading to kinematics matching the full VC^2 sample, rather than the younger emission-line dwarfs.

A possible resolution to this dilemma lies with the two component model. The observed velocity dispersions of the ultracool dwarfs are

$$(\sigma_U, \sigma_V, \sigma_W) \ = \ (32, 17, 17)$$

These values are close to the velocity dispersions that we measure for the core of both the VC^2 and faint Hipparcos samples (Table 5). We have identified those core velocity dispersions as characteristic of the Galactic disk. Are the ultracool dwarfs essentially a pure disk sample?

There are two possible explanations for the absence of thick disk dwarfs in the ultracool sample. First, the result may be due to small number statistics: there are only 37 dwarfs in the photometrically-selected sample analysed by Reid *et al.*, implying an expected number of 4 ± 2 thick disk dwarfs. Alternatively, a systematic difference in metallicity could lead to thick disk stars being intrinsically rarer amongst low-temperature, late-type dwarfs.

Expanding on the latter possibility, the location of the hydrogen-burning limit in the HR diagram is known to be a function of metallicity. This is illustrated most dramatically for extreme halo subdwarfs (e.g. NGC 6397, Bedin *et al.*, 2001), where the main-sequence terminates at $M_V \sim 15$, (V-I)~ 3, brighter and bluer than for the Galactic disk population. While the metal hydride absorption bands in those stars are consistent with late-type M dwarfs, the TiO absorption is closer to that observed in M3 dwarfs (Gizis, 1997). This behaviour is relevant because there are suggestions that the thick disk, as an old population, may have a mean metallicity $\langle [Fe/H] \rangle < -0.4$dex. This might be sufficient to move the hydrogen-burning limit to an effective spectral type of $\sim$M7, significantly reducing the contribution of thick disk dwarfs to an ultracool sample, without necessarily requiring a significant change in the underlying mass function.

We can test this hypothesis to a limited extent using data for the VC^2 sample. All of these stars have low-resolution spectroscopic observations, obtained as part of the PMSU survey. CaH and TiO band indices derived from those data can be used to provide a crude assessment of the metallicity distribution. Figure 18 plots bandstrengths for the M dwarfs in the VC^2 sample and for nearby intermediate (sdM, $\bar{[}Fe/H] \sim -1$) and extreme (esdM, $[Fe/H] < -1.5$) subdwarfs from Gizis (1997). We fit mean relations to the VC^2 stars

$$\langle CaH2 \rangle \ = \ 0.128 + 0.714 TiO5 - 0.205 TiO5^2 + 0.266 TiO5^3$$

and the intermediate subdwarfs,

$$CaH2_{sdM} \ = \ -0.219 + 2.632 TiO5 - 4.149 TiO5^2 + 2.656 TiO5^3$$

The middle panel plots the raw residuals,

$$\delta CaH2 \ = \ CaH2_{obs} \ - \ \langle CaH2 \rangle$$

as a function of W velocity; the lowermost panel plots the normalised residuals,

$$\delta CaH2_N \;=\; (CaH2_{obs} - \langle CaH2 \rangle)/(CaH2_{sdM} - \langle CaH2 \rangle)$$

If thick disk dwarfs have systematically lower metallicities than disk dwarfs, one might expect a systematic trend in the residuals with increasing velocity. There is no evidence for such behaviour in these data. However, the uncertainties in the abundance calibration are obviously substantial, and could well obscure systematics at the expected level of ~ 0.4 dex. A similar analysis of a volume-complete sample of G dwarfs, where abundances can be derived to higher accuracy, would be instructive.

6. Conclusions

In the first paper of this series (PMSU1), we used spectroscopic observations of stars in the pCNS3 to define a volume-limited sample of M dwarfs with absolute magnitudes in the range $8 < M_V < 14$, the VC sample. In the present paper, we have examined the effects of using Hipparcos distance estimates and adding newly-discovered M dwarfs which meet the relevant distance limits. The revised sample, the VC^2 sample, includes 548 main-sequence stars in 448 systems, and shows no evidence for systematic bias against stars with low space motions.

Using the revised sample, we have recomputed the stellar luminosity function, $\Phi(\mathrm{M}_V)$. We have combined those measurements with Hipparcos data for brighter stars within 25 parsecs of the Sun to derive the luminosity function for main sequence stars with $-1 < M_V < 17$, making explicit allowance for potential unseen binary companions. The results are in good agreement with Kroupa's (2001) analysis for $\mathrm{M}_V < 10$, but we derive lower space densities for mid- and late-type M dwarfs.

We have transformed the observed luminosity function to a mass function using both empirical and semi-empirical mass-M_V calibrations, with the latter taken from Kroupa, Tout & Gilmore (1993). The resulting present-day mass functions are in broad agreement, consistent with power-law distributions with $\alpha \sim 1.2$ at low masses ($M < 0.6 M_\odot$) and $\alpha \sim 5$ at high masses ($M > 1.1 M_\odot$). The semi-empirical mass-M_V relation leads to a steepening in $\psi(M)$ ($\alpha \sim 2.2$ for $0.6 < \frac{M}{M_\odot} < 1.1$. Data for additional binary stars with masses in the range $0.8 < \frac{M}{M_\odot} < 1.2$ would be useful in resolving this discrepancy. However, there is little impact on the the mass density derived by integrating $\psi(M)$; both analyses indicate that main-sequence stars contribute 0.030 to 0.033 $M_\odot pc^{-3}$ to the total mass density in the Solar Neighbourhood.

We have converted the observed present-day mass function to estimates of the initial

mass function by allowing for stellar evolution effects at high masses, and by integrating the density distribution perpendicular to the Plane. We also apply a 10% correction to allow for the presence of thick disk dwarfs in the local sample. The derived IMFs have a near-Salpeter slope at high masses, $\alpha \sim 2.5 - 2.8$, but are relatively flat at low masses, $\alpha \sim 1.1 - 1.3$.

We also consider the kinematics of Solar Neighbourhood stars. Analysis shows that both the M dwarfs in the VC^2 sample and the fainter stars ($4 < M_V < 8$) in the Hipparcos 25-parsec dataset have similar velocity distributions. This is not unexpected, since both should include representatives from the full star formation history of the Galactic Disk. Both the brighter Hipparcos stars and the dMe dwarfs amongst the VC^2 sample have cooler kinematics, as expected for datasets with younger average ages. Detailed analysis of the U- and W-velocity distributions for the two older samples shows that both are well represented by two-component Gaussians, with approximately 10% of the stars in the higher-velocity component. We identify the latter as the local component of the thick disk. A comparable analysis of a well-defined sample of solar-type stars offers the potential for obtaining insight into the detailed properties of this Galactic component.

Finally, we suggest that the thick disk component may provide an explanation for the surprisingly low velocity dispersions measured for a photometrically-selected sample of ultracool dwarfs: if the thick disk is slightly metal-poor, the hydrogen-burning limit could lie close to the M7 boundary of the ultracool sample. As a result, the coolest M dwarfs may represent a pure disk sample, a conclusion supported by the agreement between their kinematics and the core velocity dispersions measured for the FGK and early/mid-type M dwarfs in our analysis.

This research was supported partially by a grant under the NASA/NSF NStars initiative, administered by the Jet Propulsion Laboratory, Pasadena. We have made extensive use of the Simbad database, maintained by Strasbourg Observatory, and of the ADS bibliographic service.

REFERENCES

Andersen, J. 1991, Astr. Ast. Rev. **3**, 91

Bedin, L.R., Anderson, J., King, I.R., Piotto, G. 2001, ApJL 560, L75

Beuzit, J.-L., Ségransan, D., Forveille, T., *et al.*, 2001, A&A, in press

Binney, J., Dehnen, W., Bertelli, G. 2000, MNRAS, 318, 658

Chabrier, G., Baraffe, I. 2000, ARA&A, 38

Chabrier, G. 2002, ApJ, 567, 304

Dehnen, W. & Binney, J. J. 1998, MNRAS, 298, 387

Delfosse, X., Forveille, T., Beuzit, J.-L., Udry, S., Mayor, M., Perrier, C. 1999, A&A, 344, 897

Delfosse, X., Forveille, T., Ségransan, D., Beuzit, J.-L., Udry, S., Perrier, C., Mayor, M. 2000, A&A, 364, 217 (D00)

Duquennoy, A., Mayor, M., 1991, A&A, 248, 485

ESA, 1997, The Hipparcos Catalogue

Evans, D.S. 1979, IAU Symposium 30, 57

Fabricius, C., Makarov, V.V., 2000, A&AS, 144, 45

Fischer, D.A., Marcy, G.W. 1992, ApJ, 396, 178

Giclas, H.L., Burnham, R., & Thomas, N.G. 1971, The Lowell Proper Motion Survey (Lowell Observatory, Flagstaff, Arizona)

Gilmore, G.F., Reid, I.N. 1983, MNRAS, 202, 1025

Gizis, J.E. 1997, AJ, 113, 806

Gizis, J.E., Reid, I.N., Hawley, S.L. 2002, AJ, 123, 3356 (PMSU3)

Gliese, W. 1969, Catalogue of Nearby Stars, Veroff. Astr. Rechen-Instituts, Heidelberg, Nr. 22 (CNS2)

Gliese, W., Jahreiß, H. 1979, A&AS 38, 423

Gliese, W., & Jahreiß, H. 1991, Preliminary Version of the Third Catalog of Nearby Stars, ADC/CDS Catalog V/70 (pCNS3)

Hawley, S.L., Gizis, J.E., & Reid, I.N. 1996, AJ, 112, 2799 (PMSU2)

Hawley, S.L., Gizis, J.E., & Reid, I.N. 1997, ADC/CDS Catalog III/198.

Haywood, M., Robin, A.C., Crézé, M. 1997, A&A, 320, 440

Henry, T.J., McCarthy, D.W. 1993, ApJ, 350, 334

Henry, T. J., Ianna, P. A., Kirkpatrick, J. D., & Jahreiss, H. 1997, AJ, 114, 388

Henry, T.J., Franz, O.G., Wasserman, L.H., *et al.*, 1999, ApJ, 512, 864

Hillenbrand, L.A., Carpenter, J.M. 2000, ApJ, 540, 236

Jahreiß, H., Wielen, R. 1997, Proc. ESA Symp. 402, *Hipparcos - Venice '97*, ESA Publications, Noordwijk, p. 675

Kroupa, P., Tout, C.A., Gilmore, G.F. 1993, MNRAS, 262, 545

Kroupa, P. 2001, MNRAS, 322, 231

Kuijken, K., Gilmore, G. 1989, MNRAS, 239, 605

Luhman, K.L., Rieke, G.H., Young, E.T., Cotera, A.S., Chen, H., Rieke, M.J. ,Schneider, G., Thompson, R.I. 2000, ApJ, 540, 1016

Lutz, T.E., Upgren A.R. 1980, AJ, 85, 573

Luyten, W.J. 1979, Catalogue of stars with proper motions exceeding 0".5 annually (LHS), (University of Minnesota, Minneapolis, Minnesota)

Luyten W. J., 1980, New Luyten Catalogue of Stars with Proper Motions Larger than Two Tenths of an Arcsecond, (Minneapolis, University of Minnesota), computer-readable version on ADC Selected Astronomical Catalogs Vol.1 - CD-ROM

Miller, G. E. & Scalo, J. M. 1979, ApJS, 41, 513

Murray, A.C. 1983, Vectorial Astronomy (Adam Hilger, Ltd., Bristol)

Nidever, D.L., Marcy, G.W., Butler, R.P., Fischer, D.A., Vogt, S.S. 2002, ApJ, subm.

Reid, I.N., Cruz, K. 2002, AJ, 123, 2806

Reid, I.N., Cruz, K., Laurie, S., Liebert, J., Dahn, C.C., Harris, H.C. 2002a, ApJ, subm

Reid, I.N., & Gizis, J.E. 1997, AJ, 113, 2246

Reid, I.N., Hawley, S.L., & Gizis, J.E. 1995, AJ, 110, 1838 (PMSU1)

Reid, I.N., Kirkpatrick, J.D., Liebert, J., Burrows, A., Gizis, J.E., Burgasser, A., Dahn, C.C., Monet, D., Cutri, R., Beichman, C.A., & Skrutskie, M 1999, ApJ, 521, 613 (R99)

Reid, I.N., Kirkpatrick, J.D., Liebert, J., Gizis, J.E., Dahn, C.C., Monet, D.G. 2002b, AJ, in press

Salim, S., Gould, A. 2002, ApJ, in press

Salpeter, E. E. 1955, ApJ, 121, 161

Schaller, G., Schaerer, D., Meynet, G., & Maeder, A. 1992, A&AS, 96, 269

Schmidt, M. 1968, ApJ, 151, 393

Ségransan, D., Delfosse, X., Forveille, T., Beuzit, J.-L., Udry, S., Perrier, C., Mayor, M. 2000, A&A, 364, 665

Siegel, M.H., Majewski, S.R., Thompson, I.B., Reid, I.N. 2002, AJ, in press

Upgren, A.R., Grossenbacher, R., Penhallow, W.S., MacConnell, D.J., & Frye, R.L. 1972, AJ, 77, 486

Vyssotsky, A.N. 1956, AJ, 61, 201

Weis, E.W. 1986, AJ, 91, 626

Weis, E.W. 1987, AJ, 92, 451

Weis, E.W. 1988, AJ, 96, 1710

Weis, E.W., 1996, AJ, 112, 2300

Wielen, R. 1974, Highlights of Astronomy, ed. G. Contopoulos, (Reidel Publ. Co., Dordrecht),3 ,395

Wielen, R. 1977, A&A, 60, 263

Wielen, R., Jahreiß, H., Krüger, R., 1983, IAU Colloquium 76, ed. A.G. Davis Philip & A.R. Upgren, p. 163 (Davis-Philip Press, Schenectady)

Wilson, R.E. 1953, *General Catalogue of Stellar Radial Velocities*, Carnegie Inst. of Washington, D.C., Publ. 601

Table 1. Distance Limits

M_V	d_{orig} (pc)	d_{lim} (pc)
8.5	22	22
9.5	20	18
10.5	14	14
11.5	14	14
12.5	14	14
13.5	10	10
14.5	10	10
15.5	5	5

Note. — d_{orig} lists the distance limit adopted in PMSU1 d_{lim} lists the distance limit adopted in the present analysis

Table 2. Basic data for the VC sample

NN	Name	distance pc.	Ref.	M_V	V_r kms^{-1}	μ_α $''yr^{-1}$	μ_δ $''yr^{-1}$	U kms^{-1}	V kms^{-1}	W kms^{-1}	Hα Å	Comments
7	Gl 2	11.5± 0.1	1	9.63	0.4	0.879	-0.163	-39.4	-23.3	-16.6	-0.40	
11	Gl 4 A	11.8± 0.4	1	8.61	3.3	0.821	-0.172	-38.7	-20.0	-17.7	-0.57	
19	GJ 1002	4.6± 0.0	2	15.42	-40.1	-0.817	-1.870	36.7	-39.5	26.1	0.11	94/6
41	GJ 1005 A	5.6± 0.2	1	12.84	-25.5	0.625	-0.595	-6.8	-27.4	19.5	-0.22	
43	Gl 12	12.5± 0.9	2	12.10	49.6	0.618	0.319	-51.8	24.8	-29.4	-0.33	85/15
54	Gl 14	15.0± 0.1	1	8.12	3.0	0.553	0.100	-37.3	-14.7	0.6	-0.57	
60	Gl 15 A	3.6± 0.0	1	10.32	11.5	2.882	0.415	-49.3	-12.7	-2.8	-0.34	
62	Gl 16	16.2± 0.5	1	9.85	-45.4	0.000	-0.020	10.7	-27.3	34.7	-0.4	low-res
65	GJ 1008	20.8± 0.6	1	8.65	-18.2	-0.094	-0.259	21.8	-22.0	10.6	-0.4	low-res
87	Gl 21	16.3± 0.3	1	9.45	-1.1	-0.145	-0.179	10.3	6.9	-12.9	-0.40	
89	GJ 1012	12.1± 0.8	2	11.77	-13.4	-0.330	-0.805	40.9	-31.4	-2.4	-0.32	73/27
92	Gl 22 A	9.9± 0.2	1	10.39	-4.9	1.732	-0.237	-66.8	-44.9	-16.7	-0.21	
96	LP525-39	11.8± 3.5	2	12.34	-4.6	0.174	-0.067	-6.9	-11.5	0.4	5.23	0/100
115	Gl 26	12.5± 0.2	2	10.58	-0.6	1.560	0.046	-79.0	-48.0	-1.0	-0.37	91/9
165	LTT10301A	12.0± 1.2	1	12.31	6.2	0.215	-0.046	-12.1	-4.0	-5.8	4.07	
171	Gl 40 A	15.2± 0.3	1	8.04	16.5	0.622	-0.278	-27.4	-40.3	-17.6	-0.67	
187	Gl 46	13.1± 0.4	1	11.18	14.6	1.273	-0.287	-55.8	-59.4	-11.6	-0.38	
193	Gl 47	10.9± 0.3	2	10.64	8.7	0.315	-0.779	-19.5	-3.8	-39.6	-0.22	91/9
195	Gl 48	8.1± 0.0	1	10.48	0.5	1.749	-0.346	-57.3	-36.3	-9.5	-0.40	
199	Gl 49	10.1± 0.1	1	9.55	-5.0	0.683	0.068	-23.9	-22.6	5.0	-0.28	
203	V003	21.6± 1.9	1	8.36	8.9	-0.007	0.131	-8.4	13.0	-4.6	-0.68	
204	Gl 51	8.9± 0.6	2	13.92	-7.3	0.721	0.095	-20.6	-23.2	5.7	10.36	78/22
213	Gl 52	15.1± 0.2	1	8.10	4.1	1.541	0.330	-90.7	-59.4	31.4	-0.67	
234	Gl 54.1	3.8± 0.0	1	14.17	27.6	1.191	0.625	-28.6	-0.7	-23.1	1.16	
283	LHS 142	17.7± 0.5	1	9.97	-28.4	-0.542	-0.913	86.7	-32.6	12.4	-0.4	low-res
296	Gl 63	11.4± 0.9	2	10.91	-17.0	-0.164	-0.362	15.8	-11.2	-19.4	-0.24	79/21
301	Gl 65 A	2.6± 0.0	2	15.47	22.0	3.321	0.562	-41.0	-19.3	-12.3	7.86	96/4
316	LHS1289	20.8± 0.8	1	8.80	-3.6	0.552	-0.022	-38.4	-37.0	11.6	-0.62	
319	Gl 70	11.2± 0.2	1	10.68	-26.4	-0.424	-0.749	47.4	-22.8	-3.7	-0.31	
326	G271-149	13.6± 3.9	2	12.32	54.3	0.396	-0.177	-33.2	-18.0	-48.0	-0.32	0/100
342	Gl 79	11.1± 0.1	1	8.68	13.0	0.832	0.007	-35.8	-28.3	-1.8	-0.54	
350	Gl 82	12.0± 0.5	1	11.80	-8.5	0.291	-0.196	-8.2	-19.2	-5.9	6.66	
358	Gl 83.1	4.5± 0.0	2	14.02	-29.5	1.117	-1.774	13.9	-51.6	3.5	1.58	96/4
359	G244-047	9.1± 2.6	2	11.23	-83.8	-0.265	-0.118	61.9	-56.8	-11.4	-0.26	0/100
371	Gl 84	9.4± 0.1	1	10.32	25.1	1.290	-0.154	-45.2	-43.2	-8.2	-0.30	
376	Gl 84.2A	19.1± 1.9	2	8.88	63.2	0.271	-0.432	-63.0	10.3	-45.3	-0.41	75/25

Table 2—Continued

NN	Name	distance pc.	Ref.	M_V	V_r kms^{-1}	μ_α $''yr^{-1}$	μ_δ $''yr^{-1}$	U kms^{-1}	V kms^{-1}	W kms^{-1}	Hα Å	Comments
381	G173-039	13.6± 4.1	2	11.80	-10.1	0.272	-0.272	-6.6	-24.3	-9.1	4.95	0/100
390	Gl 87	10.4± 0.1	1	9.98	-3.1	-1.788	-1.885	104.7	-11.8	-72.9	-0.41	
427	Gl 96	11.9± 0.1	1	9.02	-37.9	0.220	0.050	19.8	-31.4	14.7	-0.49	
435	Gl 98 A	16.6± 0.3	1	8.26	7.9	0.143	0.211	-19.5	6.2	6.7	-0.56	
453	Gl 102	10.0± 0.7	2	12.96	-6.7	0.038	-0.686	10.0	-24.5	-20.2	2.53	82/18
461	Gl 104	14.0± 0.3	1	9.94	-1.8	0.233	-0.140	-6.3	-17.0	0.7	-0.44	
492	Gl 109	7.6± 0.1	1	11.20	29.6	0.845	-0.372	-39.3	-17.2	-12.0	-0.30	
512	Gl 116	14.2± 0.3	1	8.78	-49.7	0.931	-0.967	5.2	-102.8	-5.9	-0.48	
538	LTT1445 A	6.4± 1.9	1	11.93	-3.4	-0.343	-0.268	12.9	1.7	-4.1	0.93	
548	Gl 122	21.3± 0.4	1	8.18	33.8	0.212	-0.513	-61.6	1.0	-22.2	-0.66	
550	Gl 123	14.8± 0.3	1	8.25	-30.0	0.391	-0.912	35.2	-67.0	4.2	-0.60	
556	GJ 1054 A	16.4± 4.8	1	9.17	93.9	-0.353	-0.129	-12.6	-20.8	-95.3	1.90	
559	Gl 125	15.4± 0.9	1	9.21	-2.8	-0.428	-0.329	15.5	6.9	-35.7	-0.49	
574	GJ 1057	8.5± 0.3	2	14.15	27.0	1.703	0.107	-58.0	-41.2	19.9	-0.12	91/9
582	Gl 130.1A	14.0± 0.7	1	10.19	21.3	0.474	-0.353	-41.1	-17.2	-2.8	-0.44	
587	Gl 133	13.7± 0.3	1	10.51	-11.1	0.383	0.302	6.2	-21.5	25.0	-0.40	
590	Gl 134	17.3± 0.5	1	9.09	-5.8	0.484	-0.602	-18.4	-58.6	-16.5	-0.50	
627	Gl 143.1	21.7± 0.9	1	8.31	14.0	0.073	-0.271	5.0	-27.9	-15.1	-0.59	
663	Gl 150.1A	17.2± 0.5	1	8.79	33.6	0.103	-0.282	-27.2	-18.5	-25.5	-0.53	
677	Gl 154	14.6± 0.3	1	8.79	36.0	0.359	-0.199	-41.6	-17.8	-7.3	-0.47	
688	Gl 155.1	17.4± 0.7	1	9.84	13.9	-0.382	-0.380	16.2	-3.7	-43.5	-0.4	low-res
692	GJ 1065	9.8± 0.3	2	12.83	-10.1	-0.413	-1.367	50.8	-31.6	-30.3	-0.26	92/8
701	Gl 156	15.4± 0.2	1	8.08	62.3	-0.022	0.531	-66.3	15.7	-27.4	-0.65	
702	Gl 156.1	17.3± 3.1	1	9.67	-18.9	0.297	-0.349	-3.1	-41.5	-6.2	-0.53	
721	LHS1630	10.9± 3.3	2	12.21	-2.9	0.195	-0.629	23.0	-25.0	3.0	-0.44	0/100
724	Gl 162	13.7± 0.3	1	9.50	38.2	0.560	0.129	-48.1	-7.1	22.1	-0.42	
732	Gl 164	12.6± 1.1	2	12.99	-24.6	-0.366	-0.833	11.5	-27.4	-51.7	-0.25	73/27
780	Gl 169.1A	5.5± 0.0	1	12.39	26.8	1.374	-1.947	-55.8	-38.1	-4.0	-0.17	
799	Gl 172	10.2± 0.1	1	8.57	33.5	0.317	-0.457	-42.1	-8.9	-0.6	-0.49	
802	G039-029	10.5± 3.0	2	12.43	27.6	0.362	-0.051	-31.0	-9.5	6.2	4.81	0/100
803	Stph 497	16.5± 4.8	2	9.50	20.1	0.000	0.000	-16.5	-5.6	-10.1	1.88	0/100
804	Gl 173	11.1± 0.1	1	10.13	-5.7	-0.233	-0.217	14.4	2.0	-10.1	-0.41	
817	Gl 176	9.4± 0.2	1	10.12	26.5	0.706	-1.075	-23.6	-57.3	-11.9	-0.40	
835	GJ 1073	13.0± 0.4	2	12.86	101.8	1.190	-1.118	-125.1	-68.8	10.7	-0.06	90/10
836	Gl 179	12.1± 0.5	1	11.55	-9.1	0.160	-0.300	13.1	-17.0	1.9	-0.30	
838	Gl 180	12.4± 0.2	1	10.44	-31.6	0.452	-0.617	42.4	-22.5	26.8	-0.37	

Table 2—Continued

NN	Name	distance pc.	Ref.	M_V	V_r kms^{-1}	μ_α $''yr^{-1}$	μ_δ $''yr^{-1}$	U kms^{-1}	V kms^{-1}	W kms^{-1}	Hα Å	Comments
847	Gl 181	16.5± 0.3	1	8.69	-36.0	0.106	-0.113	28.9	-24.7	-2.0	-0.47	
854	Gl 184	14.0± 0.3	1	9.19	66.3	1.294	-1.510	-112.8	-93.7	17.7	-0.44	
855	LHS1723	7.5± 2.2	2	12.72	41.4	-0.542	-0.551	-18.6	-19.0	-42.0	1.16	0/100
856	Gl 185 A	8.5± 0.1	1	8.80	-12.4	-0.159	-0.264	16.9	4.6	-1.5	-0.50	
859	LHS1731	9.3± 0.2	1	11.85	13.3	-0.194	-0.462	6.9	-14.5	-20.2	-0.36	
874	Stph 546A	11.8± 3.4	2	9.92	23.7	0.000	0.000	-14.8	-13.7	-12.5	2.41	0/100
876	G085-041	12.8± 3.7	2	11.24	20.1	0.098	-0.270	-17.2	-18.4	-8.7	-0.16	0/100
882	Gl 190	9.3± 0.1	1	10.47	33.9	0.546	-1.263	14.7	-66.1	-15.5	-0.26	
883	G096-021	13.9± 4.2	2	10.68	13.9	0.193	-0.411	-23.6	-22.7	-4.1	-0.40	0/100
888	Gl 192	13.9± 1.0	1	10.05	-25.9	0.262	0.236	20.8	4.6	27.4	-0.40	
895	Gl 195 A	13.0± 0.4	2	9.62	32.7	0.070	-0.409	-38.9	-12.4	-7.9	-0.43	89/11
919	Gl 203	10.3± 0.3	1	12.42	59.4	-0.204	-0.756	-43.2	-38.6	-40.4	-0.12	
924	GJ 2043 A	17.4± 0.5	1	9.42	-2.6	-0.090	-0.177	6.3	-7.5	-13.4	-0.53	
930	Gl 205	5.7± 0.0	1	9.19	7.8	0.768	-2.099	23.1	-55.4	-10.1	-0.40	
933	Gl 206	13.0± 0.5	1	10.95	17.2	-0.234	-0.176	-12.1	-5.2	-21.1	3.70	
938	G097-052A	10.9± 3.3	2	12.13	-14.1	-0.111	-0.363	19.5	-8.4	-11.5	0.09	0/100
941	G097-054	11.8± 0.8	2	11.44	35.1	-0.120	-0.392	-28.0	-21.5	-22.7	0.13	77/23
943	LHS5109	11.9± 3.6	2	12.43	28.4	0.148	0.462	-38.5	-0.6	8.4	-0.02	0/100
944	Gl 208	11.4± 0.1	1	8.53	21.6	-0.015	-0.055	-19.7	-7.2	-6.1	-0.16	
956	Gl 212	12.5± 0.2	1	9.27	4.3	0.020	-0.495	-16.1	-21.7	-12.2	-0.39	
958	Wo 9188	21.5± 1.1	1	8.95	27.5	0.077	-0.045	-25.7	-13.4	0.9	-0.4	low-res
959	Gl 213	6.0± 0.1	1	12.65	105.6	2.015	-1.597	-88.5	-92.5	10.0	-0.22	
961	Gl 215	13.7± 0.1	1	8.34	-19.4	0.198	-0.814	-12.6	-53.6	-17.4	-0.57	
980	Gl 220	17.7± 1.4	2	9.57	32.3	0.115	-0.599	-27.6	-50.9	-17.4	-0.50	73/27
981	Gl 221	20.1± 0.6	1	8.18	22.0	0.000	-0.333	0.1	-33.3	-19.6	-0.61	
991	G192-011A	13.6± 3.9	1	9.59	2.0	-0.018	-0.252	-9.8	-11.2	-6.9	-0.23	
998	LHS1805	7.6± 0.2	2	12.30	2.5	-0.146	-0.818	-17.5	-19.0	-15.3	-0.16	94/6
999	G099-049	5.4± 0.2	2	12.66	28.7	0.229	-0.074	-24.4	-16.2	-0.6	3.33	91/9
1004	LHS1809	9.3± 0.2	2	14.62	19.2	0.077	-0.797	-30.1	-25.5	-7.7	-0.23	92/8
1005	Gl 226	9.4± 0.1	1	10.62	-1.1	-0.016	-1.337	-46.8	-34.3	-13.6	-0.38	
1019	Gl 228 A	10.8± 0.5	1	10.41	54.2	0.071	-0.967	-34.8	-60.2	-23.9	-0.32	
1021	Gl 229 A	5.8± 0.0	1	9.35	4.4	-0.131	-0.725	12.2	-11.8	-11.9	-0.51	
1042	Gl 232	8.4± 0.1	2	13.44	-13.5	0.563	-0.514	18.9	-25.8	9.1	-0.29	96/4
1048	Gl 234 A	4.1± 0.0	1	13.05	14.3	0.707	-0.703	-2.3	-23.5	4.5	3.42	
1057	Gl 239	10.4± 0.2	1	9.55	-58.3	-0.812	0.351	43.9	47.6	-33.2	-0.40	
1068	G108-021A	12.2± 3.5	2	11.62	81.3	0.035	-0.285	-63.5	-53.1	-5.6	-0.31	0/100

Table 2—Continued

NN	Name	distance pc.	Ref.	M_V	V_r kms^{-1}	μ_α $''yr^{-1}$	μ_δ $''yr^{-1}$	U kms^{-1}	V kms^{-1}	W kms^{-1}	Hα Å	Comments
1089	LHS 221 A	10.6± 0.2	1	10.92	-31.0	0.533	-1.016	7.8	-65.0	0.4	-0.31	
1094	Gl 251	5.8± 0.1	1	11.21	21.7	-0.753	-0.396	-27.1	-3.6	-16.5	-0.27	
1104	Gl 254	18.6± 0.6	1	8.36	-14.0	0.088	-0.213	15.5	-18.8	-3.9	-0.60	
1120	LHS 224 A	8.9± 0.2	2	14.26	23.2	0.723	-0.915	-25.0	-39.8	27.3	-0.19	89/11
1131	G250-034	17.7± 0.5	1	9.94	-5.5	-0.268	-0.077	-6.6	-0.2	-23.1	-0.41	
1138	Gl 268A	5.9± 0.1	1	13.35	32.7	-0.492	-0.930	-38.5	-19.5	-8.7	1.40	
1148	Gl 268.3A	12.3± 0.2	1	10.67	-14.4	-0.029	-0.238	13.7	-9.7	-10.9	-0.20	
1154	G107-061	14.4± 0.4	1	9.53	11.2	-0.276	-0.049	-17.5	2.9	-13.3	-0.39	
1160	Gl 270	19.8± 0.8	1	8.59	-68.1	0.465	-0.337	78.3	-37.1	4.5	-0.46	
1164	Gl 272	16.2± 0.5	1	9.49	-27.2	-0.161	-0.229	15.7	-16.3	-26.3	-0.25	
1168	Gl 273	3.8± 0.0	1	11.97	17.1	0.575	-3.717	17.3	-65.4	-17.5	-0.30	
1175	GJ 1097	11.0± 0.2	1	11.22	-0.4	0.457	-0.821	32.2	-36.9	0.7	-0.41	
1183	Gl 277 Aa	11.6± 0.3	1	10.25	0.1	-0.344	-0.274	-8.8	-9.2	-20.6	1.25	
1191	Gl 277.1	11.5± 0.2	1	10.18	-40.8	-0.420	-0.060	20.9	-12.4	-40.0	-0.42	
1193	V499	13.1± 0.4	1	10.77	-15.0	-0.097	0.037	10.9	-0.1	-12.1	-0.62	
1201	G089-032	7.1± 2.1	2	13.95	24.6	0.203	-0.290	-13.6	-22.4	7.5	4.84	0/100
1207	LHS1935	10.9± 0.3	1	11.52	-29.5	0.455	-0.507	45.0	6.4	7.0	-0.18	
1210	Gl 281	14.9± 0.3	1	8.75	24.3	-0.114	-0.245	-14.6	-25.5	-9.7	-0.65	
1219	Gl 285	5.9± 0.1	1	12.34	23.2	-0.399	-0.453	-17.6	-20.5	-9.7	8.37	
1226	GJ 1101	12.8± 0.4	2	12.55	6.7	-0.275	-0.585	-35.6	-17.3	-3.8	3.90	91/9
1233	GJ 1103 A	9.0± 0.2	2	13.73	36.0	0.254	-0.723	-6.6	-48.1	3.7	-0.31	93/7
1247	GJ 1105	8.2± 0.2	1	12.43	-21.1	0.200	-0.655	19.1	-26.8	-8.4	-0.25	
1271	Stph 681	18.8± 5.5	2	8.83	-13.5	0.000	0.000	11.5	3.3	-6.3	-0.42	0/100
1278	LHS5133 A	17.1± 0.7	1	9.04	79.4	-0.308	-0.350	-73.4	-48.2	5.5	-0.61	
1280	GJ 1108 A	20.7± 1.2	1	8.47	12.7	-0.054	-0.212	-13.1	-21.1	-2.6	1.53	low-res
1290	Gl 299	6.8± 0.1	2	13.65	12.6	1.163	-5.079	71.2	-149.5	-30.7	-0.29	96/4
1293	Gl 300	6.1± 0.3	2	13.17	7.6	0.031	-0.706	11.3	-16.1	-9.4	-0.19	86/14
1294	Gl 301 A	21.6± 1.7	1	8.06	14.1	-0.250	-0.497	10.8	-36.0	-45.0	-0.56	
1299	GJ 2066	9.1± 0.1	1	10.30	62.4	-0.367	0.045	-53.0	-35.5	9.0	-0.36	
1324	Gl 308.1	19.1± 0.6	1	8.93	-85.2	0.487	-0.714	66.1	-94.7	-6.9	-0.4	low-res
1328	GJ 2069 Aa	12.8± 0.9	1	12.05	-32.1	-0.256	-0.119	17.4	7.1	-31.2	4.60	
1337	LHS 250	13.3± 0.4	2	11.06	22.1	-0.808	-0.606	-61.4	-19.1	-20.1	-0.17	89/11
1340	Gl 310	13.9± 0.1	1	8.59	11.3	-1.065	0.037	-49.1	13.9	-49.5	-0.56	
1358	Gl 317	10.3± 2.0	2	11.93	87.8	-0.476	0.799	-74.5	-61.0	22.2	-0.28	55/45
1361	Gl 319 A	14.9± 0.4	1	8.83	25.2	0.203	-0.641	8.4	-52.7	6.3	-0.57	
1377	Gl 322	16.5± 0.3	1	8.19	-21.4	0.098	0.103	22.3	-1.9	-8.9	-0.56	

Table 2—Continued

NN	Name	distance pc.	Ref.	M_V	V_r kms^{-1}	μ_α $''yr^{-1}$	μ_δ $''yr^{-1}$	U kms^{-1}	V kms^{-1}	W kms^{-1}	Hα Å	Comments
1379	Gl 323 A	20.0± 3.2	1	8.43	-11.8	-0.060	0.000	4.1	6.9	-10.4	-0.36	
1385	Gl 325 A	11.3± 0.3	3	8.43	44.9	-1.340	-0.354	-83.4	8.2	-22.4	-0.58	
1391	Gl 328	20.0± 0.8	1	8.49	0.4	0.061	-1.064	50.7	-77.4	-40.6	-0.62	
1395	Gl 330	16.4± 0.8	1	9.52	-8.6	-0.035	-0.333	13.2	-17.9	-16.0	-0.33	
1405	G041-014Aa	5.6± 1.6	2	12.87	-6.4	0.329	-0.320	13.2	-3.9	-0.2	2.20	0/100
1417	G234-053	10.4± 0.6	2	12.56	-25.2	0.216	0.359	29.7	4.5	-12.5	-0.29	83/17
1420	G046-017	12.3± 3.6	2	11.36	49.0	-0.376	-0.080	-41.0	-34.5	6.1	-0.33	0/100
1426	Gl 334	14.5± 0.3	1	8.70	40.2	-0.305	0.220	-41.6	-21.3	9.8	-0.42	
1439	Gl 336	21.2± 1.3	1	8.33	10.1	-0.322	-0.552	-23.2	-56.3	-22.7	-0.56	
1451	Gl 338 A	6.2± 0.1	1	8.67	12.1	-1.558	-0.579	-42.7	-15.0	-22.1	-0.56	
1460	LTT3412	14.4± 4.3	2	9.96	15.5	-0.302	0.154	-26.3	-8.6	-2.7	-0.08	0/100
1465	Stph 762	20.0± 3.2	3	8.13	6.5	0.000	0.000	-4.4	-1.6	4.5	-0.66	
1501	GJ 1125	10.1± 0.3	1	11.68	44.1	-0.590	-0.526	-29.7	-49.6	-5.1	-0.33	
1507	Gl 352 A	10.5± 0.4	1	10.69	9.5	0.729	0.059	21.7	-3.9	30.5	-0.33	
1509	Gl 353	13.5± 0.3	1	9.53	20.8	-0.208	-0.546	-19.8	-37.5	5.4	-0.40	
1522	Gl 357	9.0± 0.1	1	11.16	-33.4	0.168	-0.899	37.4	13.2	-32.7	-0.32	
1527	Gl 360	11.8± 0.4	1	10.21	6.0	-0.666	-0.291	-35.9	-14.9	-13.4	-0.04	
1528	Gl 361	11.4± 0.2	1	10.09	12.5	-0.621	-0.184	-28.4	-17.7	-16.1	-0.35	
1529	Gl 362	11.5± 0.2	1	10.91	5.2	-0.666	-0.291	-34.6	-14.9	-13.5	1.09	
1530	Gl 363	14.0± 1.3	2	11.78	13.0	-0.735	-0.502	-48.4	-33.5	-13.9	-0.30	73/27
1537	Gl 366	15.9± 0.3	1	9.62	-26.2	0.117	-0.984	-0.1	-74.6	26.4	-0.41	
1541	GJ 1129	11.6± 3.4	2	12.27	7.9	-1.624	-0.171	-64.5	-20.4	-59.5	-0.14	0/100
1550	Gl 369	12.1± 1.0	1	9.63	60.8	1.068	-1.438	75.6	-89.9	21.5	-0.45	
1554	Gl 372	15.7± 0.3	1	9.55	24.0	-0.090	-0.462	3.4	-41.8	-6.7	-0.38	
1558	Gl 373	10.5± 0.1	1	8.89	16.9	-0.302	-0.585	-25.7	-22.7	13.4	-0.45	
1575	Gl 378	14.9± 0.3	1	9.21	-6.9	-0.634	-1.437	-26.5	-107.2	-13.0	-0.51	
1586	LHS2224	13.5± 0.5	2	12.81	43.9	-0.454	-0.808	-47.7	-47.3	30.6	-0.25	89/11
1587	Gl 379 A	21.2± 1.1	1	8.55	-51.6	0.224	0.267	52.3	-2.8	-33.9	-0.52	
1592	Gl 380	4.9± 0.0	1	8.16	-21.9	-1.357	-0.523	-11.9	-20.6	-32.5	-0.61	
1594	Gl 381A	12.3± 0.2	1	10.90	27.0	0.510	-0.653	34.5	-40.2	16.0	-0.37	
1595	Gl 382	7.8± 0.1	1	9.81	8.9	-0.157	-0.232	-3.1	-13.2	-1.7	-0.30	
1596	Gl 383	17.1± 0.3	1	8.78	-2.5	-0.525	0.001	-34.0	-5.4	-25.1	-0.55	
1605	GJ 2079	20.4± 0.6	1	8.65	4.9	-0.094	-0.210	-3.0	-22.1	-4.7	0.83	
1611	Gl 386	13.7± 0.4	1	10.29	-9.9	-0.415	-0.618	1.8	-21.3	-44.5	0.37	
1616	Gl 388	4.9± 0.0	2	10.96	11.1	-0.503	-0.053	-14.2	-7.3	2.6	3.40	95/5
1630	Gl 390	12.5± 0.2	1	9.69	22.7	-0.718	0.077	-42.1	-23.4	-5.3	-0.41	

Table 2—Continued

NN	Name	distance pc.	Ref.	M_V	V_r kms^{-1}	μ_α $''yr^{-1}$	μ_δ $''yr^{-1}$	U kms^{-1}	V kms^{-1}	W kms^{-1}	Hα Å	Comments
1642	Gl 393	7.2± 0.1	1	10.34	8.8	-0.587	-0.746	-6.9	-29.1	-15.2	-0.53	
1649	Gl 397.1A	17.5± 0.3	1	8.72	-2.9	-0.144	0.206	-9.0	12.3	-14.5	-0.52	
1657	LHS 283	12.5± 0.6	2	11.45	-50.4	-1.652	-0.585	-57.1	-77.1	-64.2	-0.22	79/21
1658	Gl 398	13.4± 0.7	2	11.97	19.7	-0.636	0.090	-42.3	-16.2	-2.0	4.40	82/18
1664	GJ 1134	10.3± 0.2	2	12.91	-2.0	-1.461	-0.362	-55.0	-35.5	-33.5	-0.30	92/8
1671	Gl 400 A	14.1± 0.4	1	8.55	-1.8	-0.037	0.156	-3.8	9.4	-3.9	-0.45	
1682	GJ 1138 A	9.8± 0.3	2	13.05	58.2	-0.674	-1.030	-39.2	-58.1	41.7	-0.27	89/11
1687	Gl 402	6.9± 0.2	1	12.46	-2.5	-0.815	-0.812	-10.0	-27.8	-23.4	-0.28	
1690	Gl 403	13.0± 2.1	2	12.10	19.2	-1.110	0.188	-69.1	-17.3	-10.1	-0.14	65/35
1692	LHS2320	9.9± 2.9	2	14.41	0.2	-0.625	-0.135	-22.2	-13.6	-14.9	6.84	0/100
1709	Gl 408	6.6± 0.1	1	10.91	3.2	-0.402	-0.233	-9.1	-11.4	-3.0	-0.31	
1717	Gl 410	11.7± 0.1	1	9.26	-14.2	0.140	-0.059	12.5	3.3	-10.2	0.00	
1719	Gl 411	2.5± 0.0	1	10.47	-85.9	-0.569	-4.773	46.1	-52.4	-75.8	-0.20	
1723	Gl 412 A	4.8± 0.0	1	10.30	69.6	-4.427	0.949	-122.8	-5.9	18.7	-0.26	
1732	Gl 413.1	10.7± 0.1	1	10.30	-4.5	-0.793	-0.449	-24.0	-19.5	-34.6	-0.59	
1742	G119-062	13.3± 3.9	2	11.76	3.6	-0.178	0.098	-13.1	1.8	-1.2	4.20	0/100
1746	Stph 928	14.4± 4.2	2	9.97	30.0	0.000	0.000	-7.9	-9.1	27.5	-0.50	0/100
1756	Gl 421 A	16.6± 1.2	1	8.86	9.1	0.140	-0.741	38.7	-34.1	-30.7	-0.72	
1762	GJ 1144	17.6± 0.4	1	8.78	-7.8	-0.206	-0.096	-11.2	-4.8	-16.5	-0.4	low-res
1765	GJ 1145	17.6± 0.4	1	8.57	-19.1	0.157	-0.100	12.7	17.5	-11.7	-0.58	
1770	Gl 424	9.1± 0.0	1	9.51	61.0	-2.955	0.186	-141.0	-11.7	-1.2	-0.44	
1801	Gl 430.1	16.2± 0.3	1	9.25	-5.9	-0.580	0.000	-37.6	-15.9	-18.7	-0.31	
1810	LHS2427	17.8± 0.5	1	9.93	-35.0	-0.622	-0.278	-41.1	-3.7	-53.1	-0.4	low-res
1827	GJ 1148	11.0± 0.3	1	11.68	-9.8	-0.600	-0.119	-22.0	-19.6	-15.7	-0.27	
1830	Gl 436	10.2± 0.2	1	10.62	7.6	0.757	-0.770	46.4	-19.6	15.6	-0.37	
1845	Gl 445	5.4± 0.0	1	12.16	-112.2	0.711	0.489	67.2	-54.7	-74.6	-0.23	
1847	G010-049A	13.9± 4.2	2	12.54	6.9	-0.290	-0.089	-13.8	-16.0	-1.3	4.66	0/100
1849	Gl 447	3.3± 0.0	1	13.50	-31.0	0.633	-1.190	17.3	5.9	-32.8	-0.18	
1854	GJ 1151	8.3± 0.2	2	13.66	-35.6	-1.536	-0.978	-27.5	-67.5	-33.1	-0.13	93/7
1855	Gl 450	8.6± 0.1	1	10.07	1.0	-0.220	0.272	-12.7	6.2	-2.4	-0.26	
1866	Gl 452.1	12.1± 1.8	2	12.35	3.5	0.083	-0.781	25.7	-35.9	-9.5	1.25	70/30
1894	G237-043	12.7± 3.8	2	12.56	4.4	-0.474	-0.067	-25.7	-13.7	1.1	-0.18	0/100
1905	LHS2520	10.1± 2.9	2	12.04	79.5	-0.050	-0.718	31.1	-73.3	34.2	-0.26	0/100
1907	LTT4562 A	12.8± 0.4	1	11.13	-9.1	-0.198	-0.160	-8.8	-4.6	-14.9	-0.30	
1915	Gl 458 A	15.3± 0.3	1	8.86	-19.9	0.230	0.082	18.8	6.1	-17.9	-0.58	
1923	GJ 1154 A	8.4± 0.3	2	14.11	-13.7	-0.942	-0.288	-28.5	-20.4	-22.3	5.41	90/10

Table 2—Continued

NN	Name	distance pc.	Ref.	M_V	V_r kms^{-1}	μ_α $''yr^{-1}$	μ_δ $''yr^{-1}$	U kms^{-1}	V kms^{-1}	W kms^{-1}	Hα Å	Comments
1934	GJ 1156	6.6± 0.1	2	14.70	5.1	-1.285	0.206	-37.8	-16.0	2.0	6.11	95/5
1937	Gl 461 A	15.2± 4.6	2	9.19	4.0	0.088	-0.020	6.7	0.3	3.6	-0.35	0/100
1938	Gl 462	16.0± 0.3	1	8.42	22.6	0.163	-0.523	24.0	-23.9	33.0	-0.59	
1942	G237-064	13.0± 0.9	1	10.68	14.9	0.208	-0.120	7.8	8.9	17.4	-0.23	
1943	Gl 464	21.2± 0.8	1	8.75	7.6	0.026	-0.186	12.1	-16.1	2.8	-0.72	
1945	Gl 465	8.9± 0.2	1	11.54	51.5	1.082	-2.289	94.4	-65.6	-28.9	-0.28	
1952	LTT4730 A	13.4± 4.0	2	10.33	-6.9	-0.281	0.015	-17.5	-4.6	-6.2	0.57	0/100
1954	Gl 469	13.6± 0.5	1	11.39	-10.2	-0.638	-0.288	-27.0	-32.5	-18.8	-0.33	
1966	Gl 471	13.4± 0.3	1	9.06	15.1	-0.635	-0.533	-15.7	-52.5	0.7	-0.38	
1972	Gl 473 A	4.3± 0.0	2	14.85	2.4	-1.796	0.233	-33.4	-15.8	1.6	4.78	95/5
2009	Gl 486	8.2± 0.2	1	11.80	19.1	-0.990	-0.424	-20.7	-39.0	13.0	-0.28	
2017	Gl 487 Aa	10.2± 0.1	1	12.05	-16.0	-0.427	-0.091	-10.0	-22.5	-9.8	0.20	
2024	Gl 488	10.8± 0.1	1	8.33	6.7	-0.039	-0.400	9.9	-18.9	-3.7	-0.65	
2043	Gl 493.1	8.4± 0.3	2	13.78	-25.5	-0.942	0.242	-42.1	-6.4	-18.4	4.59	92/8
2045	Gl 494 A	11.4± 0.1	1	9.46	-12.2	-0.714	-0.021	-33.4	-20.4	-10.3	1.09	
2051	Gl 499 A	18.6± 0.7	1	8.09	1.2	-0.059	0.060	-7.1	1.3	2.2	-0.33	
2093	Gl 507 A	13.2± 0.5	1	8.91	-15.1	0.374	-0.789	48.2	-27.7	-11.2	-0.47	
2096	Gl 507.1	17.4± 0.7	1	9.42	-13.2	-0.217	-0.125	-8.5	-20.7	-9.9	-0.54	
2097	Gl 508 Aa	10.4± 0.2	1	9.50	1.9	0.144	-0.028	6.3	3.9	1.4	-0.46	
2100	Gl 508.2	16.1± 0.3	1	9.59	-39.8	0.518	-0.288	43.6	-0.5	-41.6	-0.46	
2102	LHS 350	13.5± 0.4	2	12.28	-18.4	-0.629	-0.878	-1.1	-69.7	-16.0	-0.25	87/13
2107	Gl 509 A	18.5± 0.6	1	8.18	-38.3	-0.486	0.234	-49.6	-13.0	-32.8	-0.59	
2112	Gl 510	16.3± 0.5	1	9.95	-29.8	-0.460	-0.103	-42.9	-7.2	-17.9	0.01	
2123	Gl 514	7.6± 0.1	1	9.64	15.2	1.111	-1.084	57.2	-8.6	-3.5	-0.43	
2128	G165-008A	10.5± 3.2	2	12.20	-7.5	-0.228	-0.159	-4.8	-14.0	-5.3	9.00	0/100
2137	GJ 1172	20.5± 0.6	1	8.41	13.7	0.139	-0.132	22.1	-4.4	5.0	-0.57	
2150	Gl 519	10.9± 0.1	1	8.86	-14.4	0.309	-0.060	13.4	4.3	-16.6	-0.53	
2151	Gl 520 A	21.9± 1.1	1	8.47	-21.1	-0.211	-0.112	-7.7	-29.5	-11.4	-0.49	
2156	Gl 521	13.3± 0.3	1	9.62	-60.7	-0.047	0.399	-15.2	-5.9	-63.7	-0.44	
2157	Gl 521.1	14.5± 0.3	1	8.78	28.8	-0.384	0.495	-22.1	-0.6	46.8	-0.56	
2168	LHS2784	9.1± 0.2	1	12.16	6.6	-0.106	-0.700	16.7	-24.4	10.1	-0.21	
2173	Gl 525	13.0± 0.1	1	9.23	18.9	0.436	-1.845	93.3	-72.4	-7.6	-0.44	
2175	LHS2794	11.4± 0.5	1	11.57	5.0	-0.313	-0.538	-0.5	-31.2	-13.4	-0.28	
2176	Gl 526	5.4± 0.0	1	9.79	16.0	1.786	-1.488	61.5	-2.0	-3.3	-0.45	
2198	Gl 532	14.0± 0.1	1	8.17	-46.5	0.423	-0.147	30.5	-8.5	-45.2	-0.58	
2201	Gl 533 A	20.9± 0.6	1	8.25	-10.5	-0.174	-0.673	22.1	-62.0	-22.8	-0.76	

Table 2—Continued

NN	Name	distance pc.	Ref.	M_V	V_r kms^{-1}	μ_α $''yr^{-1}$	μ_δ $''yr^{-1}$	U kms^{-1}	V kms^{-1}	W kms^{-1}	Hα Å	Comments
2204	GJ 1181 A	16.8± 0.7	1	8.47	13.9	-0.248	-0.095	-3.9	-24.3	6.1	-0.62	
2214	LHS2836	11.4± 3.4	2	12.71	-15.8	-0.553	-0.185	-28.6	-18.3	-9.3	4.01	0/100
2216	Gl 536	10.2± 0.1	1	9.66	-25.3	-0.784	0.611	-54.0	3.4	4.4	-0.51	
2222	Gl 537 A	11.4± 0.5	2	9.57	-42.2	0.583	-0.046	24.4	1.4	-46.7	-0.30	87/13
2235	Gl 540	16.3± 0.8	1	9.29	16.2	0.219	-0.534	30.0	10.0	35.4	-0.49	
2241	Wo 9472	19.6± 0.6	1	8.70	-10.4	0.160	0.149	-1.6	22.2	-5.0	-0.4	low-res
2259	Gl 541.2	18.6± 0.4	1	8.90	4.4	0.038	-0.016	3.5	3.1	3.2	-0.51	
2268	Gl 545	11.8± 1.4	2	12.54	53.2	-0.612	-0.868	28.9	-71.0	22.0	-0.23	72/28
2278	Gl 548 A	16.8± 0.3	1	8.63	8.7	0.789	-1.127	104.8	-23.1	-23.6	-0.60	
2295	Gl 552	14.3± 0.4	1	9.91	6.0	-1.058	1.345	-100.9	21.7	53.2	-0.44	
2299	Gl 553	16.5± 0.3	1	8.32	-22.6	-1.263	-0.225	-72.1	-72.5	11.2	-0.70	
2300	Gl 553.1	11.1± 0.3	1	11.69	0.5	-0.393	-0.367	-6.4	-27.3	-3.7	-0.28	
2310	Gl 555	6.1± 0.1	1	12.39	-1.9	-0.342	0.599	-13.6	6.2	13.4	-0.18	
2313	Gl 558	20.4± 0.4	1	8.03	-46.2	-0.753	0.232	-73.6	-48.0	-14.8	-0.4	low-res
2316	LHS2952	13.9± 4.2	2	11.02	-26.6	0.619	-0.663	61.9	-9.3	-19.1	0.90	0/100
2329	Wo 9492	9.9± 1.2	1	10.86	21.1	-0.328	-0.052	-11.7	2.5	23.3	-0.36	
2340	Gl 563.2A	4.2± 0.4	1	13.52	-39.6	-1.201	-0.197	-44.8	-3.3	-11.6	-0.4	low-res
2356	Gl 568 A	10.2± 0.6	1	12.14	-36.2	-0.684	0.105	-37.5	-27.6	-16.0	0.20	
2358	Gl 569 A	9.8± 0.1	1	10.25	-6.9	0.318	-0.106	8.4	5.1	-13.9	0.85	ref
2359	LHS2998	11.0± 3.3	2	12.11	-40.4	0.156	-0.823	27.8	-37.7	-36.6	-0.30	0/100
2378	Gl 571.1	19.5± 0.6	1	8.03	14.3	0.009	-0.470	26.2	-33.4	-17.1	-0.73	
2379	LHS3012	13.8± 4.0	2	12.04	-17.3	-0.494	-0.091	-25.4	-27.1	-0.3	-0.43	0/100
2381	Gl 572	11.7± 0.1	1	8.78	-11.1	0.232	0.319	-8.5	12.5	-19.3	-0.41	
2390	Gl 576	19.2± 0.6	1	8.40	-83.3	-0.569	-0.483	-56.8	-72.0	-56.0	-0.81	
2392	LHS3018	17.6± 0.4	1	9.77	-24.7	-0.659	0.187	-41.4	-46.5	1.9	-0.29	
2397	Gl 579	16.8± 1.2	2	8.97	-70.7	-0.873	0.494	-96.0	-41.4	-21.3	-0.60	83/17
2419	LHS3056	11.0± 3.3	2	12.37	-29.1	-0.694	-0.206	-38.4	-27.9	-4.0	-0.30	0/100
2420	Gl 581	6.3± 0.1	1	11.56	-10.3	-1.189	-0.290	-22.7	-29.3	8.0	-0.36	
2427	Gl 583	18.9± 0.4	1	8.25	-19.0	-0.298	0.008	-28.1	-16.7	2.6	-0.63	
2428	Wo 9520	11.4± 0.2	1	9.83	7.4	0.083	0.119	1.4	9.6	4.7	1.86	
2458	Gl 592	12.9± 0.6	2	12.14	1.5	-0.457	-0.625	-0.5	-47.0	-5.8	-0.42	84/16
2464	Gl 595	9.6± 0.9	1	11.96	78.6	-2.012	-1.016	38.0	-107.1	61.5	-0.21	
2472	Gl 597	13.1± 0.3	1	11.64	-42.2	0.824	-0.790	76.4	-2.1	-31.1	-0.19	
2504	Gl 606	13.9± 0.3	1	9.78	-17.0	0.188	-0.049	-8.6	5.0	-18.8	-0.34	
2516	Gl 609	9.9± 0.3	2	12.57	5.7	-0.959	-1.245	29.4	-64.6	20.9	-0.20	90/10
2543	V759	17.1± 0.2	1	9.03	-18.8	0.217	0.075	-1.4	0.2	-26.4	-0.38	

Table 2—Continued

NN	Name	distance pc.	Ref.	M_V	V_r kms^{-1}	μ_α $''yr^{-1}$	μ_δ $''yr^{-1}$	U kms^{-1}	V kms^{-1}	W kms^{-1}	Hα Å	Comments
2563	Gl 616.2	20.7± 0.4	1	8.39	-27.5	0.191	-0.454	46.2	-19.7	-23.7	1.93	
2566	Gl 617 A	10.7± 0.1	1	8.47	-18.4	-0.502	0.091	-10.1	-29.7	4.6	-0.63	
2576	Gl 619	15.9± 0.2	1	8.25	5.8	-0.026	0.119	-6.9	6.3	5.5	-0.67	
2578	Gl 620	16.8± 0.5	1	9.10	-30.3	-0.317	-0.638	-31.4	-51.1	-23.1	-0.49	
2582	Gl 622	17.9± 0.5	1	9.14	-63.1	-0.558	-0.313	-69.7	-45.4	-2.1	-0.43	
2583	Gl 623	8.0± 0.0	1	10.74	-23.7	1.145	-0.453	24.4	5.2	-46.1	-0.24	
2589	Gl 625	6.6± 0.0	1	11.03	-12.0	0.399	-0.130	6.4	-1.9	-16.5	0.03	
2599	Gl 628	4.3± 0.0	1	11.94	-21.3	-0.070	-1.173	-13.0	-20.7	-20.7	-0.23	
2616	Gl 630.1Aa	13.5± 0.5	2	12.25	-191.0	-1.125	1.165	-99.5	-174.0	-83.8	3.40	82/18 CM Dra
2618	LP275-68	13.3± 3.9	2	12.34	4.0	0.134	-0.144	11.7	3.5	-4.5	4.10	0/100
2642	Gl 638	9.8± 0.0	1	8.16	-31.1	-0.050	0.386	-29.8	-12.7	-15.6	-0.66	
2660	Gl 643	6.5± 0.1	1	12.75	15.2	-0.804	-0.877	19.1	-33.1	10.7	-0.23	
2661	Gl 644 A	6.5± 0.1	1	10.66	14.2	-0.795	-0.876	18.2	-33.1	10.2	1.71	
2665	GJ 1207	10.0± 0.7	2	12.29	-4.2	0.513	-0.377	7.9	-0.2	-29.4	3.30	83/17
2673	Gl 649	10.3± 0.1	1	9.59	5.6	-0.109	-0.516	22.6	-13.4	1.4	-0.49	
2674	G139-003	13.8± 4.0	2	12.43	-26.4	-0.380	0.007	-23.4	-27.0	6.2	0.99	0/100
2688	LHS3262	9.6± 0.2	2	13.66	36.9	0.145	0.629	-21.0	38.9	16.5	-0.07	93/7
2692	Gl 654	9.3± 0.8	1	10.23	34.5	-0.923	-1.132	45.7	-53.5	19.8	-0.40	
2700	Gl 655	13.5± 0.5	1	10.96	-50.3	-0.481	-0.012	-35.1	-47.4	-1.9	-0.33	
2708	G203-047A	7.6± 0.2	1	12.39	-42.8	0.333	-0.269	-1.8	-28.3	-35.5	-0.13	
2712	Gl 660 A	12.1± 0.6	1	11.64	-6.7	-0.448	-0.317	-0.6	-30.6	9.9	-0.17	
2714	LTT15087	12.0± 0.2	1	11.21	-45.2	0.232	-0.024	-14.3	-25.8	-36.8	-0.28	
2717	Gl 661 A	6.1± 0.1	1	11.02	-29.8	0.239	-1.564	36.4	-31.5	-25.7	-0.27	
2728	Stph 145	16.3± 4.7	2	9.30	-16.1	0.000	0.000	-10.7	-9.2	-7.7	-0.45	0/100
2744	Gl 669 A	10.5± 0.2	1	11.31	-35.9	-0.215	0.372	-36.4	-20.1	-4.5	1.76	
2748	Gl 671	12.4± 0.2	1	10.91	-19.3	0.298	-0.810	39.9	-20.0	-30.9	-0.39	
2756	Gl 673	7.7± 0.0	1	8.09	-23.1	-0.579	-1.181	1.1	-52.4	-9.5	-0.64	
2772	Gl 678.1	10.0± 0.1	1	9.31	-12.9	0.026	-0.261	-3.5	-13.9	-10.7	-0.46	
2789	Gl 685	14.1± 0.1	1	9.23	-14.0	0.257	-0.512	34.8	-2.8	-21.1	-0.40	
2792	Gl 686	8.1± 0.1	1	10.08	-9.6	0.932	0.992	-34.0	35.2	-20.8	-0.38	
2797	Gl 687	4.6± 0.0	1	10.85	-28.4	-0.333	-1.261	30.7	-25.1	-6.5	-0.34	
2804	V796 A	21.8± 6.3	1	8.58	-26.1	-0.045	0.052	-5.4	-24.6	-10.1	1.31	
2817	Gl 694	9.5± 0.1	1	10.59	-14.8	0.010	-0.636	22.8	-19.1	-12.4	-0.34	
2830	Gl 696	21.9± 0.9	1	8.47	-25.4	-0.027	-0.151	-17.2	-22.6	-9.6	-0.62	
2849	Gl 699	1.8± 0.0	1	13.23	-111.1	-0.755	10.282	-140.5	2.6	18.5	-0.20	
2851	LHS3343	13.6± 0.3	1	11.13	-31.9	-0.029	0.593	-44.8	-20.7	-6.7	-0.22	

Table 2—Continued

NN	Name	distance pc.	Ref.	M_V	V_r kms^{-1}	μ_α $''yr^{-1}$	μ_δ $''yr^{-1}$	U kms^{-1}	V kms^{-1}	W kms^{-1}	Hα Å	Comments
2859	Gl 701	7.8± 0.1	1	9.93	32.5	0.551	-0.333	32.7	14.1	-18.8	-0.45	
2865	GJ 1224	7.7± 0.2	2	14.20	-34.8	-0.564	-0.350	-28.9	-29.1	10.8	3.01	93/7
2882	Gl 708.2	19.0± 1.3	1	8.81	7.5	0.084	-0.494	34.6	-18.7	-23.4	-0.51	
2885	Gl 709	17.1± 0.2	1	9.12	-36.1	-0.031	0.298	-32.2	-28.3	-7.2	-0.54	
2888	LHS 462 A	11.5± 0.5	2	11.57	0.1	-0.334	-1.039	54.5	-23.8	0.0	-0.29	89/11
2892	Gl 710	19.3± 0.4	1	8.23	-13.5	-0.013	-0.005	-11.5	-7.2	-0.5	-0.60	
2897	LHS3376	7.5± 0.2	2	14.09	5.0	0.468	-0.411	11.6	14.1	-13.5	2.14	92/8
2901	LTT15435	13.0± 3.9	2	11.93	-21.8	-0.068	-0.177	-1.8	-23.7	-6.8	-0.23	0/100
2904	GJ 1227	8.3± 0.1	2	13.82	-14.4	-0.931	-1.231	53.8	-24.8	19.7	-0.17	96/4
2916	G205-028	11.9± 3.6	2	11.61	-18.2	-0.087	0.410	-26.5	-12.7	5.1	-0.15	0/100
2921	LP229-17	7.2± 2.1	2	12.14	12.4	0.046	-0.218	10.7	9.8	0.5	-0.22	0/100
2923	Gl 720 A	15.5± 0.2	1	8.90	-30.4	0.452	0.341	-37.9	-9.7	-33.5	-0.51	
2925	G141-021	11.0± 3.2	2	12.24	-43.3	0.194	0.288	-43.0	-16.4	-9.2	0.47	0/100
2928	GJ 2138	12.7± 0.4	1	10.74	-39.7	0.123	-0.530	-30.8	-37.0	-18.1	-0.30	
2933	Gl 724	16.2± 0.5	1	9.58	-32.6	-0.078	-0.666	-15.2	-57.0	-15.5	-0.50	
2935	GJ 1230 Aa	7.3± 1.2	2	13.78	-37.6	0.499	0.041	-26.2	-22.2	-23.0	2.10	55/45
2940	G206-040	11.4± 0.2	1	10.99	-30.1	-0.307	0.011	-10.8	-31.9	6.9	-0.32	
2942	G141-029	11.6± 3.4	2	12.49	-33.2	-0.044	0.310	-34.3	-14.0	5.2	4.19	0/100
2945	Gl 725 A	3.5± 0.0	1	11.19	-1.3	-1.358	1.822	-24.3	-12.7	25.9	-0.31	
2947	LTT7434	10.3± 3.0	2	12.59	-32.0	0.297	-0.318	-34.2	-12.1	-12.4	-0.34	0/100
2953	Gl 726	14.1± 0.1	1	8.10	12.4	-0.121	-0.247	19.9	-9.8	-0.7	-0.59	
2958	Gl 728	17.1± 0.3	1	8.05	-22.0	-0.413	-0.425	18.5	-48.1	11.6	-0.67	
2960	Gl 729	3.0± 0.0	1	13.08	-10.9	0.690	-0.207	-12.7	-1.1	-7.9	1.80	
2964	G205-038	13.0± 3.8	2	11.95	-76.9	0.251	-0.117	-12.6	-65.5	-41.9	-0.33	0/100
2966	Gl 731	15.6± 0.3	1	9.18	-10.5	-0.251	-0.475	22.5	-34.4	-0.4	-0.46	
2974	Gl 734 A	15.5± 1.7	2	8.49	-24.1	0.120	-0.010	-19.4	-13.7	-9.7	-0.69	69/31
2976	Gl 735	11.6± 0.2	1	9.79	-6.2	0.101	-0.082	-3.5	-5.0	-7.3	2.10	
2988	Gl 740	11.1± 0.1	1	9.00	11.2	-0.208	-1.228	48.3	-41.0	-20.0	-0.61	
3004	Gl 745 A	8.6± 0.2	1	11.09	33.0	-0.472	-0.334	35.6	13.1	14.1	-0.20	
3009	Gl 747 A	8.3± 0.1	2	12.27	-47.3	1.232	1.075	-71.4	-11.8	-33.7	-0.21	97/3
3013	G207-019	12.4± 3.7	2	11.33	-1.7	-0.220	-0.220	14.3	-10.0	5.6	-0.34	0/100
3024	Gl 748	9.6± 0.2	1	11.18	-41.4	1.733	-0.490	-47.1	-15.6	-77.2	-0.26	
3037	Gl 752 A	5.9± 0.0	1	10.27	36.3	-0.601	-1.337	54.0	-7.4	-5.1	-0.42	
3049	GJ 1236	11.2± 0.2	2	12.10	27.3	-0.740	-0.389	46.3	-7.1	22.8	-0.25	95/5
3074	Gl 763	14.5± 0.3	1	8.55	-59.8	0.523	0.303	-69.9	-15.7	-13.2	-0.55	
3100	Gl 766 A	10.9± 0.5	2	12.73	-5.6	-0.032	-1.226	47.2	-29.4	-30.9	-0.19	84/16

Table 2—Continued

NN	Name	distance pc.	Ref.	M_V	V_r kms^{-1}	μ_α $''yr^{-1}$	μ_δ $''yr^{-1}$	U kms^{-1}	V kms^{-1}	W kms^{-1}	Hα Å	Comments
3102	G125-030	11.4± 0.6	1	10.57	-16.6	0.407	0.207	-25.2	-6.7	-14.3	-0.40	
3103	Gl 767 A	13.4± 0.3	1	9.51	-4.6	0.470	-0.409	5.8	-4.9	-39.1	-0.45	
3113	GJ 1243	11.9± 0.2	2	12.45	-14.1	0.154	0.246	-18.4	-10.9	-3.0	4.94	91/9
3120	GJ 1245 Aa	4.7± 0.1	2	15.05	5.1	0.439	-0.585	7.5	5.9	-14.2	2.77	93/7
3147	GJ 1248	13.7± 0.7	2	11.41	30.8	-0.489	-0.782	64.6	-18.3	-5.3	-0.28	91/9
3177	LTT8005	20.4± 0.6	1	8.81	-6.4	0.009	-0.269	5.0	-24.7	-9.1	-0.4	low-res
3193	Gl 791	12.2± 1.2	1	10.97	-3.7	-0.199	-0.869	9.8	-50.7	-0.5	-0.41	
3195	GJ 1253	9.4± 0.3	2	14.18	-60.4	0.247	0.553	-22.3	-61.8	-7.5	-0.13	91/9
3198	Gl 791.2	8.8± 0.1	2	13.33	-28.6	0.674	0.121	-35.4	-15.7	-11.5	4.74	95/5
3203	Gl 793	8.0± 0.0	1	11.06	10.2	0.452	0.283	-20.3	8.6	-5.3	-0.04	
3224	GJ 1256	9.8± 0.2	2	13.46	-60.2	1.328	0.668	-85.9	-28.2	-14.5	0.14	93/7
3234	Gl 800 A	14.8± 1.5	1	9.99	3.8	0.647	-0.890	-9.3	-52.3	-56.1	-0.48	
3243	LTT16065	12.0± 3.6	2	12.14	-28.3	0.194	0.163	-27.3	-15.1	6.2	-0.33	0/100
3244	Gl 804	19.9± 0.6	1	8.81	4.0	0.022	-0.560	35.4	-21.5	-33.1	-0.51	
3247	Gl 806	11.8± 0.1	1	10.41	-24.2	0.423	0.278	-29.2	-21.3	-8.9	-0.43	
3263	Gl 809	7.0± 0.0	1	9.31	-17.5	-0.007	-0.772	21.9	-10.8	-19.1	-0.46	
3265	Gl 810 A	11.2± 1.0	2	12.20	-141.9	1.417	-0.447	-138.2	-83.9	15.2	-0.21	67/33
3269	Gl 812 A	13.5± 0.9	1	11.26	-42.1	0.784	-0.226	-52.7	-34.9	-22.5	2.37	
3273	Gl 813	13.6± 0.5	1	11.34	-35.3	0.759	-0.175	-37.0	-34.8	-34.4	-0.4	low-res
3278	Gl 815 A	15.1± 0.5	1	9.45	4.6	0.607	-0.278	-13.6	3.1	-45.9	2.50	
3284	Gl 816	13.8± 0.4	1	10.53	-15.1	-0.192	-0.478	12.2	-34.5	4.8	-0.36	
3307	Gl 821	12.1± 0.2	1	10.44	-56.7	0.713	-1.971	-25.2	-126.3	-33.0	-0.35	
3323	LTT16240A	12.6± 3.8	2	12.18	-4.8	0.211	0.049	-11.9	-3.8	-5.9	4.81	0/100
3360	Gl 829 A	6.7± 0.1	1	11.88	-25.1	0.993	0.365	-37.9	-17.5	-4.1	-0.27	
3363	Gl 831 A	7.8± 0.2	1	12.60	-57.5	1.194	-0.017	-63.8	-33.6	7.2	0.41	
3367	LP397-34	13.3± 3.9	2	12.04	1.2	0.232	-0.020	-13.3	-0.9	-14.8	3.10	0/100
3375	Gl 834 A	21.4± 1.5	1	8.69	2.1	-0.210	-0.158	26.6	1.2	2.0	-0.35	
3378	Gl 835	12.5± 0.4	1	9.40	-11.9	0.429	-0.023	-20.3	-13.6	-13.9	-0.45	
3398	Gl 836.8	20.3± 0.4	1	8.09	10.4	-0.051	0.061	0.0	11.4	6.0	-0.65	
3403	GJ 1263	12.1± 0.7	2	12.25	-28.2	0.760	-0.517	-31.1	-45.3	-23.7	-0.26	81/19
3452	Gl 842.2	20.9± 0.4	1	8.97	-15.0	0.225	0.024	-13.1	-17.4	-15.9	-0.55	
3453	G188-038	8.8± 0.1	1	12.28	-5.4	0.393	0.034	-14.4	-6.9	-6.7	4.84	
3454	Gl 843	12.3± 0.9	2	11.58	-23.2	0.925	0.079	-56.1	-12.3	-12.9	-0.28	78/22
3455	Gl 844	16.4± 0.5	1	9.56	-12.3	0.404	0.147	-34.1	-8.9	-5.2	-0.27	
3458	Gl 846	10.3± 0.1	1	9.12	19.4	-0.465	-0.258	31.2	7.2	-5.3	-0.52	
3466	LTT8848	21.4± 3.4	1	8.51	18.8	-0.259	-0.138	35.0	1.2	-3.3	-0.55	

Table 2—Continued

NN	Name	distance pc.	Ref.	M_V	V_r kms^{-1}	μ_α $''yr^{-1}$	μ_δ $''yr^{-1}$	U kms^{-1}	V kms^{-1}	W kms^{-1}	Hα Å	Comments
3478	Gl 849	8.8± 0.1	1	10.67	-16.2	1.037	-0.027	-40.5	-17.7	-13.5	-0.38	
3486	Gl 851	11.4± 0.1	1	9.92	-53.0	0.328	0.198	-29.3	-42.5	23.8	-0.37	
3487	Wo 9773	13.9± 0.8	1	11.28	9.1	0.092	-0.675	20.9	-22.8	-33.8	-0.4	low-res
3496	Gl 851.5	19.8± 0.6	1	8.88	17.3	-0.255	0.509	-7.2	37.4	41.3	-0.4	low-res
3517	LHS3799	7.5± 0.3	2	13.88	-2.1	0.288	-0.723	0.2	-26.1	-9.4	3.79	88/12
3526	G232-070	12.8± 3.7	2	12.37	2.2	0.133	-0.313	2.1	3.5	-20.3	-0.23	0/100
3537	Gl 860 A	4.0± 0.0	1	11.84	-34.1	-0.857	-0.393	26.0	-28.3	1.9	-0.12	
3542	GJ 1270	13.6± 0.5	2	12.59	0.0	1.203	0.474	-81.1	-13.3	-14.0	-0.19	87/13
3544	Gl 863	12.8± 0.4	1	9.83	-5.4	0.527	0.146	-32.3	-5.9	-7.3	-0.39	
3553	Gl 864	17.5± 0.5	1	8.79	8.9	0.053	-0.605	22.7	-33.4	-31.4	-0.53	
3558	G189-030	18.9± 0.6	1	8.03	-53.2	-0.028	-0.328	23.9	-55.4	-8.0	-0.66	
3559	LTT9123 A	12.3± 3.7	2	10.47	26.1	-0.014	-0.260	17.0	-9.7	-23.0	-0.36	0/100
3561	Gl 866 A	3.4± 0.0	2	15.02	-37.4	2.364	2.236	-54.9	-19.7	27.2	1.80	96/4
3562	Gl 867 A	8.6± 0.1	1	9.43	-21.2	0.456	-0.056	-23.2	-13.5	9.0	2.20	
3584	Gl 873	5.1± 0.0	1	11.76	0.0	-0.770	-0.468	21.4	3.8	-1.4	4.05	
3592	Gl 875	14.0± 0.3	1	9.12	-8.4	-0.104	0.111	0.4	3.6	12.6	-0.51	
3604	Gl 876	4.7± 0.0	1	11.79	-3.3	0.953	-0.631	-13.2	-19.7	-9.9	-0.20	
3614	Stph 206	14.6± 4.2	2	9.67	-33.2	0.000	0.000	-0.7	-26.5	20.1	-0.47	0/100
3616	Gl 880	6.9± 0.0	1	9.49	-27.1	-1.034	-0.281	32.9	-16.2	24.8	-0.42	
3621	Gl 884	8.1± 0.0	1	8.34	16.6	-0.909	0.065	34.6	17.4	-0.6	-0.58	
3629	GJ 1278	20.0± 0.4	1	8.38	8.5	0.317	-0.097	-26.2	0.4	-19.2	-0.62	
3637	Gl 889.1	15.7± 0.5	1	9.94	31.4	0.462	0.266	-36.3	22.3	-27.3	-0.39	
3641	G028-044	13.6± 3.9	2	12.00	-7.4	0.270	-0.359	-5.0	-27.6	-10.4	-0.26	0/100
3653	GJ 2154 A	16.8± 5.0	2	9.49	2.0	0.452	0.047	-32.3	-8.5	-14.0	-0.59	0/100
3672	G067-053	12.0± 3.6	2	11.70	-3.7	0.260	-0.070	-10.7	-10.1	-5.6	3.80	0/100
3686	LHS 543	10.7± 0.3	1	11.58	-7.6	-0.531	-1.384	58.1	-34.2	-34.2	-0.21	
3689	Gl 895	13.1± 0.1	1	9.44	-31.3	-0.025	-0.286	18.6	-27.1	-14.7	-0.49	
3705	Gl 896 A	6.2± 0.1	1	11.41	-0.5	0.560	-0.017	-14.1	-7.0	-4.9	4.43	
3708	Gl 897 A	12.6± 1.3	2	10.45	-0.8	0.324	-0.235	-10.7	-20.0	-7.7	1.98	70/30
3712	Gl 899	14.0± 0.8	1	10.45	-5.0	-1.028	-0.932	89.4	-21.9	-5.0	-0.37	
3713	Gl 900	19.3± 0.6	1	8.14	-10.1	0.344	0.048	-29.8	-14.9	1.7	-0.08	
3743	Gl 905	3.2± 0.0	2	14.78	-77.7	0.085	-1.615	33.5	-74.3	-0.5	0.09	98/2
3748	GJ 1289	8.1± 0.2	2	13.01	-3.7	0.926	-0.135	-28.0	-19.4	-12.0	0.53	93/7
3754	Gl 906	19.7± 0.6	1	8.43	-19.4	0.294	0.057	-20.3	-26.6	6.1	-0.62	
3759	Gl 908	6.0± 0.0	1	10.10	-72.0	0.995	-0.941	-8.5	-70.6	40.6	-0.33	
3767	LHS4022	10.6± 3.1	2	11.36	-7.4	0.584	0.325	-32.5	-6.8	8.9	-0.39	0/100

Table 2—Continued

NN	Name	distance pc.	Ref.	M_V	V_r kms^{-1}	μ_α $''yr^{-1}$	μ_δ $''yr^{-1}$	U kms^{-1}	V kms^{-1}	W kms^{-1}	Hα Å	Comments
3782	Gl 912	17.2± 3.4	1	9.96	17.1	-0.460	-0.354	46.8	0.8	-18.4	-0.37	
3786	GJ 1292	13.1± 0.4	2	11.13	-32.4	1.032	-1.032	-21.0	-84.1	-41.8	-0.24	85/15
3791	Gl 913	17.4± 0.7	1	8.43	7.6	0.642	-0.003	-49.2	-17.0	-12.4	-0.50	

Note. — Column 1 lists the identifier from the PMSU1 tables; Column 2 gives the pCNS3 name;
Column 3 lists the distance estimate and associated uncertainty - an uncertainty of $\pm$0.0km s^{-1} indicates $\epsilon_d < 0.1$ parsecs;
Column 4 gives the source of the distance estimate:
1 - trigonometric parallax from the Hipparcos catalogue (ESA, 1997)
2 - PMSU1 (Reid *et al.*, 1995). The relative weights given to trigonometric and spectroscopic parallax measurements are listed in column 13: for example, 85/15 indicates that 85% of the weight rests with π_{trig}.
3 - trigonometric parallax from pCNS3 (Jahreiss & Gliese, 1991)
Column 5 lists the visual absolute magnitude; Column 6 lists the radial velocity, usually from either PMSU3 or Delfosse *et al.*(1998), but see notes to column 13. The echelle data are accurate to $\pm$1 kms^{-1}; the low-resolution data are accurate to $\pm$10 kms^{-1}
Columns 7 and 8 give the proper motion in arcseconds/year from either Hipparcos data (column 4 = 1) or the pCNS3;
Columns 9, 10 and 11 give the derived (U, V, W) space motions;
Column 12 lists the Hα equivalent width, where, following PMSU3, a negative value indicates absorption;
Column 13 lists comments on individual stars:
the relative weights of the trigonometric/spectroscopic parallax measurements contributing to d are given (see above);
'low-res' indicates that the star has no PMSU3 echelle observations, and both the Hα equivalent width and the radial velocity are from the PMSU1 low-resolution data.

Table 3. Basic data for supplementary stars

Hip	Name	distance pc.	M_V	V_r kms^{-1}	μ_α $''yr^{-1}$	μ_δ $''yr^{-1}$	U kms^{-1}	V kms^{-1}	W kms^{-1}	Hα Å	Comments
6290	LHS 1234	19.0±1.9	8.97	22±5	-0.294	0.436	9.5	38.7	33.7		1
29052	LP 838-16	11.4±0.3	11.58	···	-0.184	-0.204	8.0	-0.4	-12.5	abs	
34361	GJ 2055	17.2±0.7	9.93	···	0.195	-0.210	17.9	-13.7	6.3	abs	
36985	G 112-29	14.3±0.3	9.09	···	0.036	-0.253	10.0	-12.9	-5.9	0.5	
38594	Ross 429	19.5±0.6	8.30	···	-0.300	0.200	-27.1	13.5	-14.0	abs	
48659	LP 847-48	11.5±0.4	11.74	···	-0.104	-0.154	0.7	-3.8	-9.3	0.3	
55605	Vys 130	16.1±6.8	9.33	70±20	0.256	-0.147	13.1	-34.4	63.7	abs	2
56157	LP 672-42	14.0±0.8	11.26	···	-0.355	0.262	-28.9	2.5	2.9	0.2	
92444	CD-27 13268	17.3±0.6	8.46	···	-0.140	-0.023	3.0	-6.1	9.4		
103039	LP 816-60	5.5±0.1	12.71	···	-0.307	0.031	4.9	0.3	6.3		
105533	BD+10 4534	20.7±0.7	8.33	···	-0.057	0.032	2.2	2.1	5.6		
110980	LP 640-74	21.9±0.9	8.81	···	0.045	-0.197	6.2	-15.9	-12.2		
114242	HD 218422	19.9±4.3	8.71	···	-0.087	-0.167	13.1	-11.8	1.8		

Note. — Astrometric and photometric data are from the Hipparcos catalogue. The Hα measurements are from unpublished spectroscopy with the CTIO 1.5-metre; as in Table 2, a positive equivalent width indicates emission.
Comments:
1. V_r from Wilson (1953);
2. V_r from Evans (1979).

Table 4. The Nearby-star Luminosity Function

	Hipparcos			PMSU4				Φ_1	Φ_{tot}
M_V	N_1	N_{c1}	N_{c2}	N_1	N_{c1}	N_{c2}	N_S	stars pc^{-3} $\times 10^4$	stars pc^{-3} $\times 10^4$
-0.5	3							0.46	0.46
0.5	5	1	1					0.76	0.92
1.5	15	2	2					2.29	2.60
2.5	36	1	1					5.50	5.65
3.5	79	9	9					12.07	13.45
4.5	151	15	15					23.07	25.36
5.5	147	19	19					22.46	25.36
6.5	181	32	32					27.65	32.54
7.5	143	24	24					21.85	25.52
8.5	8	41	27	103	7	7	6	32.01	40.16
9.5		23	13	92	7	5	3	50.21	58.26
10.5		28	4	64	15	9		74.24	88.16
11.5		21	2	66	17	11	3	76.56	91.06
12.5		15	6	71	25	17	1	82.36	107.30
13.5		7		23	14	6		73.21	92.31
14.5				13	6	3		41.38	50.93
15.5		5	1	4	12	5		101.86	248.28
16.5				1	2	2		25.46	76.39
17.5				2	6	1		50.93	76.39

Note. — Column 2 lists the number-magnitude distribution of single stars and primary stars in the Hipparcos 25-parsec sample; column 3 gives the magnitude distribution for all known companions; column 4 lists the number of companions which fall within the distance limits given in Table 1. Columns 5, 6 and 7 provide the same statistics for the PMSU4 sample, and column 8 gives the contribution from the supplementary stars listed in Table 3. Combining the samples, the luminosity function due to primaries and single stars is listed in column 9, while the space densities given in column 10 include the contribution from the companions listed in columns 4 and 7.

Table 5. Kinematics of nearby Stars

Sample		$\langle U \rangle$ kms^{-1}	$\langle V \rangle$ kms^{-1}	$\langle W \rangle$ kms^{-1}	σ_U kms^{-1}	σ_V kms^{-1}	σ_W kms^{-1}	Comment
VC[2] dM+dMe	436	-9.7	-22.4	-8.9	37.9	26.1	20.5	unweighted
					42.1	32.9	32.2	$\|W\|$ weighted
					34	18	16	core
VC[2] dMe	83	-15.4	-16.5	-10.1	25.0	21.1	17.8	unweighted
					33.6	44.6	36.1	$\|W\|$ weighted
					12	11	11	core
Hipparcos $M_V < 4$	137	-7.8	-10.0	-8.9	27.4	14.2	14.2	unweighted
					29.4	15.4	21.8	$\|W\|$ weighted
					35	18	16	core
Hipparcos $M_V \geq 4$	532	-12.7	-22.8	-6.5	39.9	27.9	19.1	unweighted
					45.2	33.4	29.2	$\|W\|$ weighted
					26	14	10	core

Note. — Unweighted: $\sigma = \Sigma((x_i - \bar{x})/n)$
$|W|$ Weighted: weighted using Wielen's prescription (see text)
core: linear fit to central regions of probability distributions (Figure 16).

Figure Captions

Fig. 1.— A comparison between distance determinations pre- and post-Hipparcos. The upper panel plots the difference, $\Delta d = d_{PMSU4} - d_{PMSU1}$, for the 1684 M dwarfs. The lower panel shows the effect on the original VC sample, plotting the revised distances and absolute magnitudes in comparison to the PMSU1 distance limits. 71 of 499 systems fall outwith the formal sampling volume.

Fig. 2.— The run of density with increasimg distance for pCNS3 M dwarfs as a function of absolute magnitude. The dotted vertical lines mark the distance limits for the volume-complete sample; the dashed vertical line for M_V=9.5 marks the value adopted in Paper I.

Fig. 3.— The distribution of the VC^2 systems on the celestial sphere, as a function of both equatorial and Galactic co-ordinates. The solid line indicates the -30° limit in both cases.

Fig. 4.— Comparison between the properties of the full VC^2 sample and the subset of stars identified in the Vyssotsky and Upgren objective prism surveys. The upper panels plot the distribution as a function of distance: the left-hand panel shows the differential number distribution, with the full sample plotted as a solid line and the spectroscopically-identified subset as a dotted line; the right-hand panel shows the fractional contribution from the spectroscopically-selected sample. The predominant contribution of the latter at larger distances is clearly illustrated. The lower panels plot the differential distribution as a function of tangential velocity, with the right-hand panel plotting the fractional contribution from the spectroscopically-selected sample. The horizontal dotted line in the latter panel indicates the fractional contribution of the latter stars to the full sample.

Fig. 5.— The (M_V, (B-V)) colour-magnitude diagram for Hipparcos stars with $\pi > 40$ mas. The four subdwarfs discussed in the text are plotted as solid triangles, while stars identified as giants or subgiants are plotted as solid points.

Fig. 6.— The (M_V, (B-V)) colour-magnitude diagram after adjusting magnitudes of close binary systems to allow for the contribution from fainter components. Solid squares mark stars in our 25-parsec sample: note that several fall below $M_V = 8$ after correction for binarity. Other symbols have the same meaning as in Figure 5.

Fig. 7.— The run of density with distance for main-sequence stars with $4 < M_V < 8$. The initial point marks the mean density within 16 parsecs for each absolute magnitude interval; subsequent points plot the density within annuli from 16 to 18, 18 to 20, 20 to 22 and 22 to 25 parsecs. There is no evidence for a significant downturn with increasing distance, indicating

a high degree of completeness in the sample.

Fig. 8.— The luminosity function for nearby stars, derived by combining data for the Hipparcos 25-parsec sample and the PMSU sample. Data for single stars and primaries are plotted as solid triangles; the open circles plot the space densities once the appropriate companions are included, with the errorbars reflecting Poisson uncertainties. The solid histogram plots $\Phi(M_V)$ from Wielen, Jahreiß & Krüger (1983).

Fig. 9.— The Duquennoy & Mayor G-dwarf sample: the lower figure compares the parallaxes listed in the CNS2 catalogue against the Hipparcos data; the upper figure plots the distribution of the stars in the (M_V, (B-V)) plane. Single stars are plotted as solid triangles, binaries as open circles. The photometry of the latter stars has been corrected to exclude contributions from secondary components.

Fig. 10.— The nearby star luminosity function, adjusted to include the contribution from "missing" binary components. The symbols have the same meaning as in Figure 8. As discussed in the text, we have doubled the contribution from known companions to the Hipparcos 25-parsec sample.

Fig. 11.— The (M_V, mass) relation for main-sequence stars: solid points and open circles plot data for primary and secondary stars, respectively, from Andersen's compilation of eclipsing binaries; solid triangles plot data for lower main-sequence binaries from Ségransan *et al.* (2000). The five-point star marks the Sun. In the left-hand panel, the long-dashed line shows the empirical fit to the upper main-sequence stars given in the text, the dotted line plots the (M_V, mass) relation derived by Delfosse *et al.* (2000) and the solid line shows the three-component fit from Henry *et al.* (1993). Ther right-hand panel compares the former two relations against the KTG semi-empirical relation (solid line).

Fig. 12.— The stellar mass function for the Solar Neighbourhood. The uppermost panel shows the results of applying the mass-luminosity relation to the dataset used to derive $\Phi(M_V)$) plotted in Figure 8, with the dotted histogram outlining the contribution from single stars and primary stars in binary systems; the middle panel shows $\xi(M)$ when double weight is given to the Hipparos 25-parsec secondaries; the lowest panel shows $\xi(M)$ for the northern 8-parsec sample (Reid *et al.*, 1999). In each case, the dashed lines plot the best-fit power-law (see text).

Fig. 13.— A comparison between the present-day mass function derived using the empirical mass-M_V calibration (upper panel) and the KTG semi-empirical calibration (lower panel). The latter includes the empirical eclipsing-binary relation for $M_V < 3.5$. As in Figure 12, the

dotted histogram plots results for single stars/primaries. The main differences lie at near-solar masses, with the semi-empirical calibration showing a steepening at $\sim 0.7M_{\odot}$ rather than $\sim 1M_{|}odot$.

Fig. 14.— The initial mass function: the upper panel shows results based on the empirical mass-M_V relation; the lower plots results using the KTG semi-empirical relation at $M_V > 3.5$. The units on the ordinate are surface density, with an arbitrary normalisation. The dashed lines mark the power-law representations described in the text. The solid line and dotted line plot log-normal functions, with the former plotting the best-fit function (see text) and the latter, the original Millar-Scalo function with C_1=1.15.

Fig. 15.— (U, V, W) diagrams for the VC^2 (right-hand panels) and Hipparcos 25-parsec (left-hand panels) datasets. Solid points mark dMe dwarfs in the VC^2 sample and Hipparcos stars with $M_V < 4.0$, respectively.

Fig. 16.— Probability plots for (U, V, W) velocity distributions. The solid line plots data for the full VC^2 sample; the long-dashed lines outline data for the 83 dmE dwarfs in the VC^2 sample; the dotted lines plot the distributions of the Hipparcos faint ($M_V > 4$) sample; and the short-dashed lines plot the bright ($M_V \leq 4$) Hipparcos dataset. The similarity between the full VC^2 and faint Hipparcos datasets is clear.

Fig. 17.— Two-component fits to probability plots of the W velocity distribution of the PMSU VC^2 M dwarf sample (upper plot) and the Hipparcos faint-star sample (lower plot). In both cases, the observations are plotted as a solid line and the low-velocity component is modelled with $\sigma_W = 16$ km s^{-1} ; the tabulated velocity distributions and relative normalisations refer to the higher-velocity component.

Fig. 18.— The uppermost panel plots the CaH2/TiO5 distribution of the VC^2 M dwarfs (squares), intermediate subdwarfs (sdM - triangles), and extreme subdwarf (esdM - open circles). The solid lines are polynomial relations matched to the first two datasets. The middle panel plots the CaH2 residuals for the VC^2 dwarfs as a function of W velocity; the lower panel plots those residuals normalised to the offset between the mean M dwarf and sdM relations. Neither of the residual plots show evidence for a systematics trend with velocity.

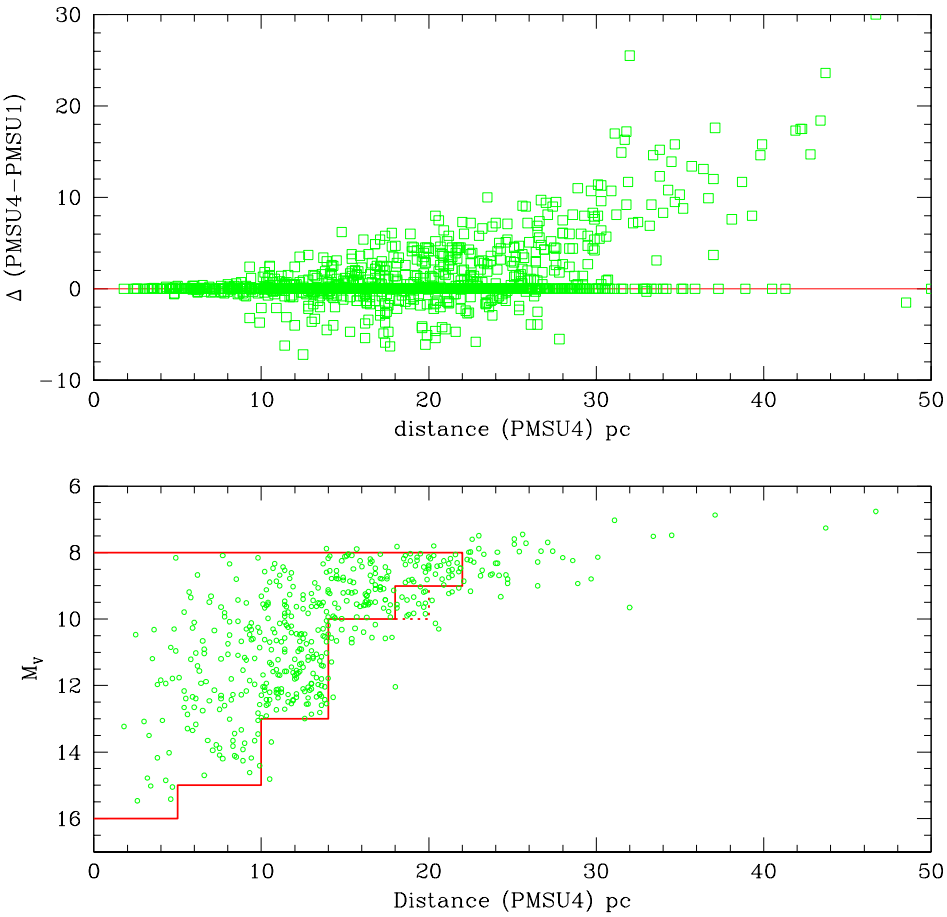

Fig. 1.— A comparison between distance determinations pre- and post-Hipparcos. The upper panel plots the difference, $\Delta d = d_{PMSU4} - d_{PMSU1}$, for the 1684 M dwarfs. The lower panel shows the effect on the original VC sample, plotting the revised distances and absolute magnitudes in comparison to the PMSU1 distance limits. 71 of 499 systems fall outwith the formal sampling volume.

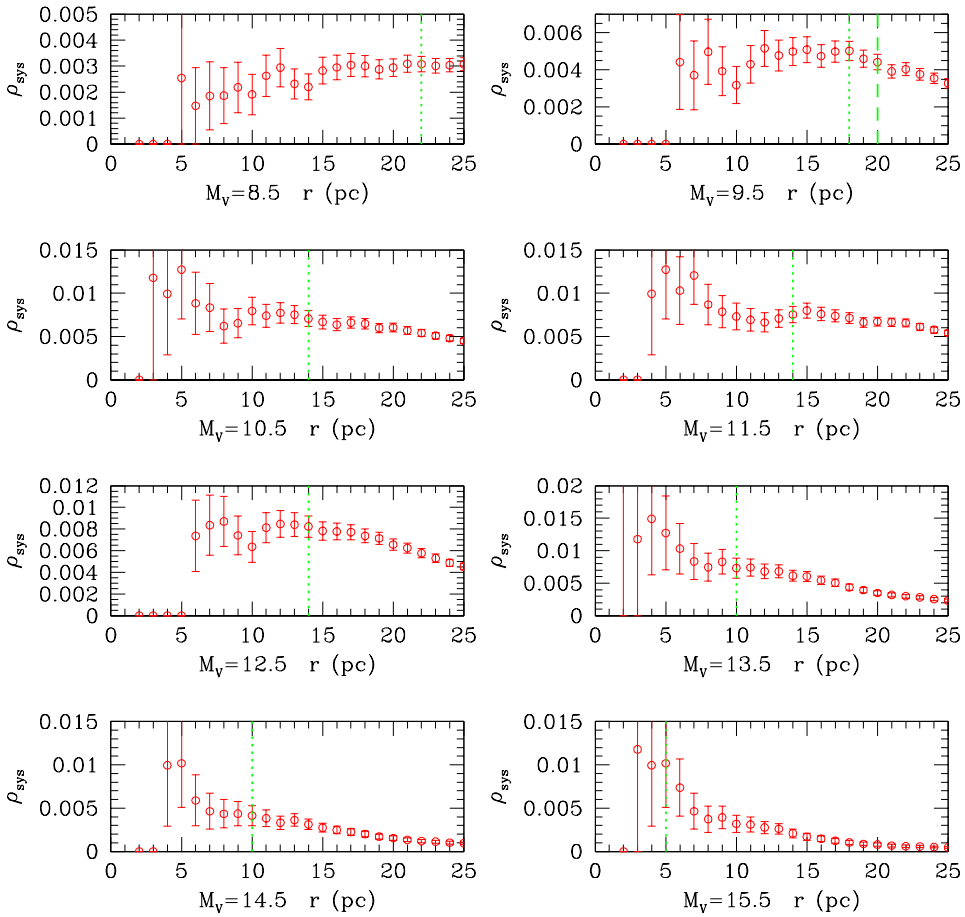

Fig. 2.— The run of density with increasimg distance for pCNS3 M dwarfs as a function of absolute magnitude. The dotted vertical lines mark the distance limits for the volume-complete sample; the dashed vertical line for M_V=9.5 marks the value adopted in Paper I.

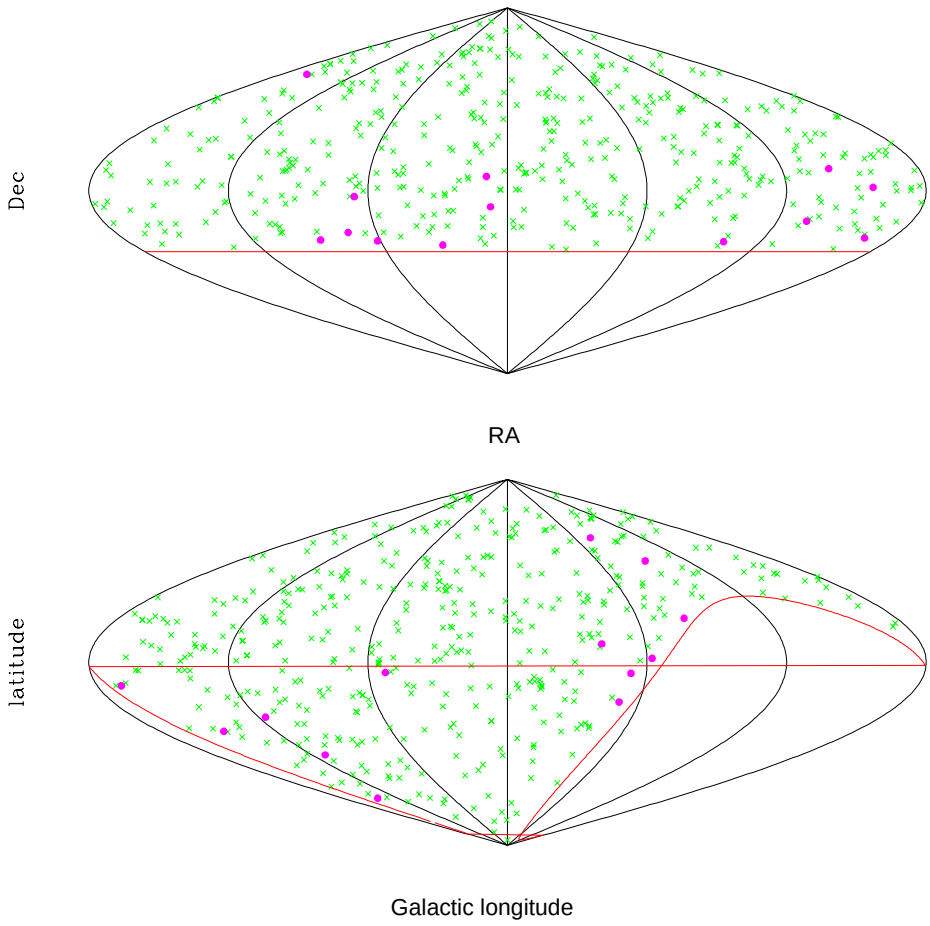

Fig. 3.— The distribution of the VC^2 systems on the celestial sphere, as a function of both equatorial and Galactic co-ordinates. The solid line indicates the $-30°$ limit in both cases.

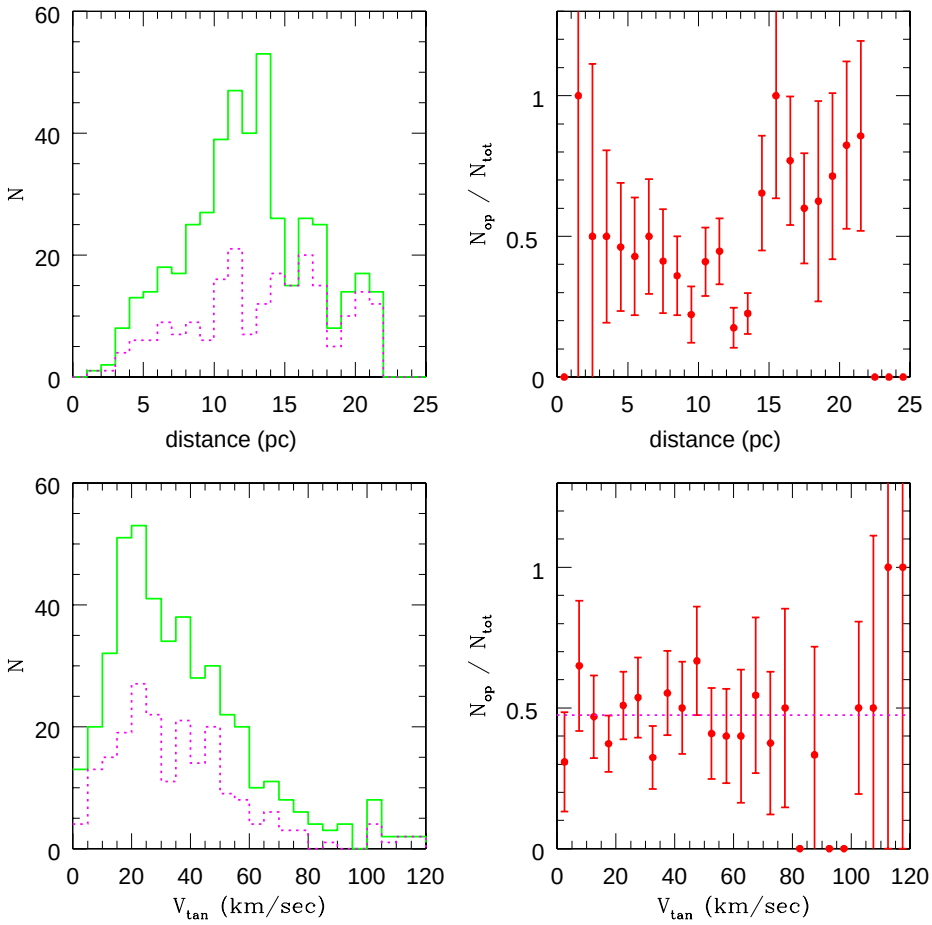

Fig. 4.— Comparison between the properties of the full VC^2 sample and the subset of stars identified in the Vyssotsky and Upgren objective prism surveys. The upper panels plot the distribution as a function of distance: the left-hand panel shows the differential number distribution, with the full sample plotted as a solid line and the spectroscopically-identified subset as a dotted line; the right-hand panel shows the fractional contribution from the spectroscopically-selected sample. The predominant contribution of the latter at larger distances is clearly illustrated. The lower panels plot the differential distribution as a function of tangential velocity, with the right-hand panel plotting the fractional contribution from the spectroscopically-selected sample. The horizontal dotted line in the latter panel indicates the fractional contribution of the latter stars to the full sample.

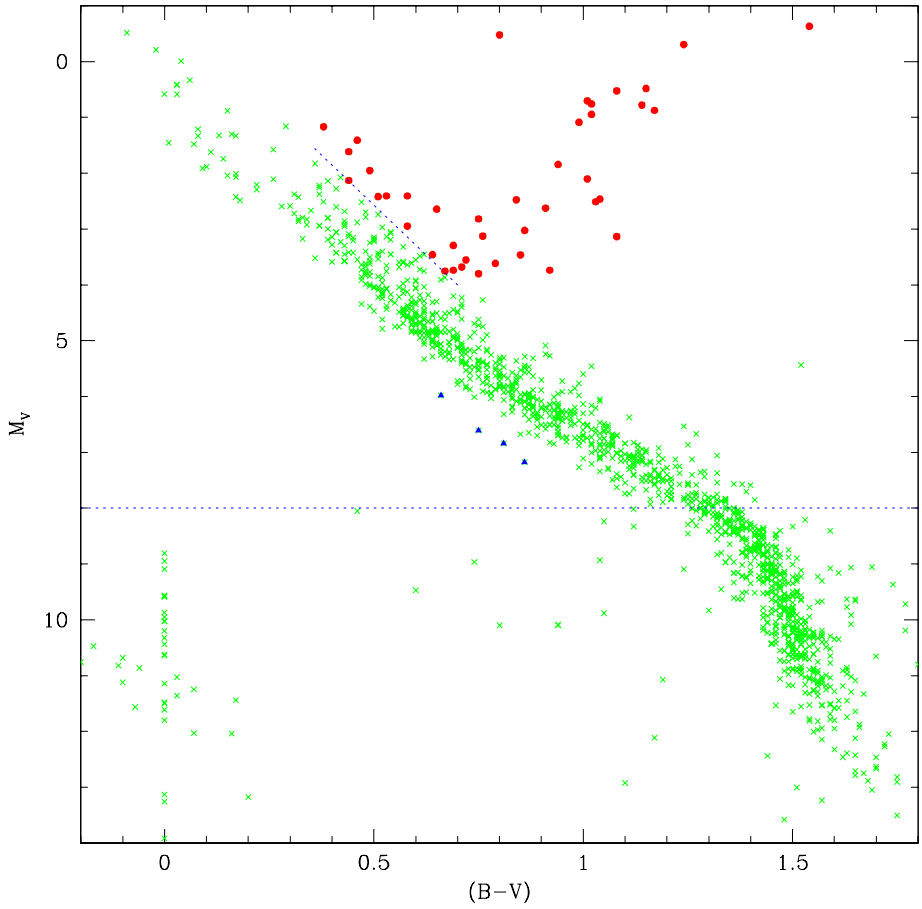

Fig. 5.— The (M_V, (B-V)) colour-magnitude diagram for Hipparcos stars with $\pi > 40$ mas. The four subdwarfs discussed in the text are plotted as solid triangles, while stars identified as giants or subgiants are plotted as solid points.

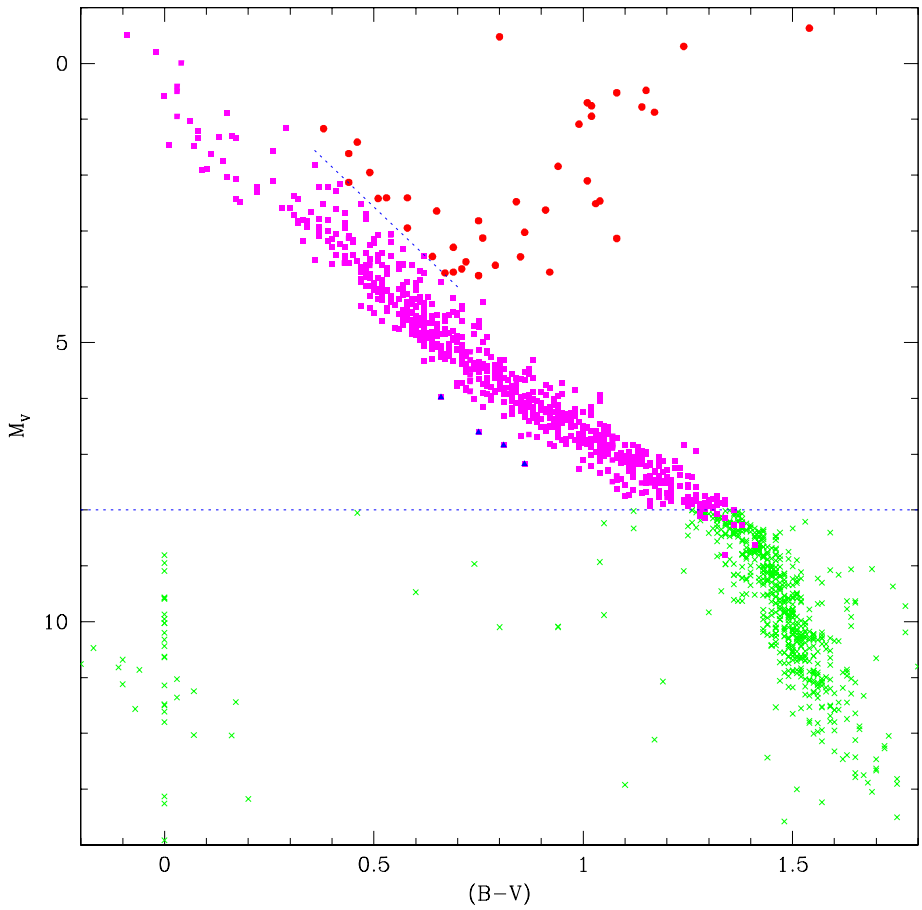

Fig. 6.— The (M_V, (B-V)) colour-magnitude diagram after adjusting magnitudes of close binary systems to allow for the contribution from fainter components. Solid squares mark stars in our 25-parsec sample: note that several fall below $M_V = 8$ after correction for binarity. Other symbols have the same meaning as in Figure 5.

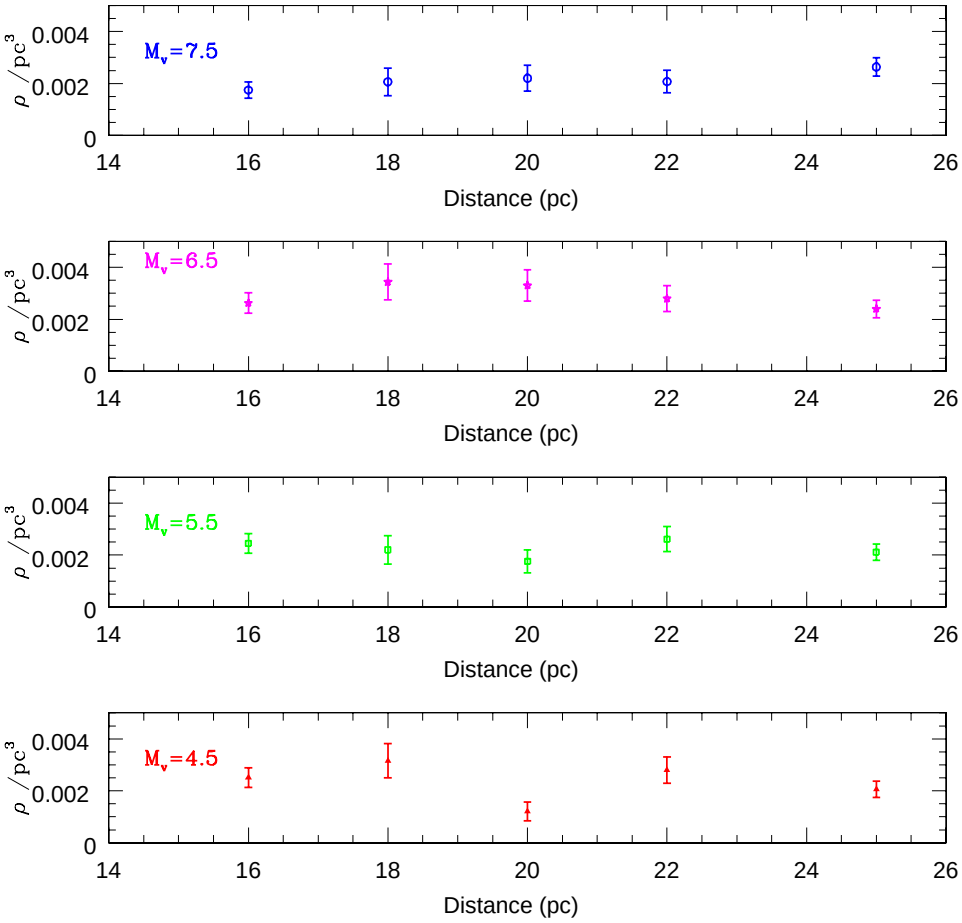

Fig. 7.— The run of density with distance for main-sequence stars with $4 < M_V < 8$. The initial point marks the mean density within 16 parsecs for each absolute magnitude interval; subsequent points plot the density within annuli from 16 to 18, 18 to 20, 20 to 22 and 22 to 25 parsecs. There is no evidence for a significant downturn with increasing distance, indicating a high degree of completeness in the sample.

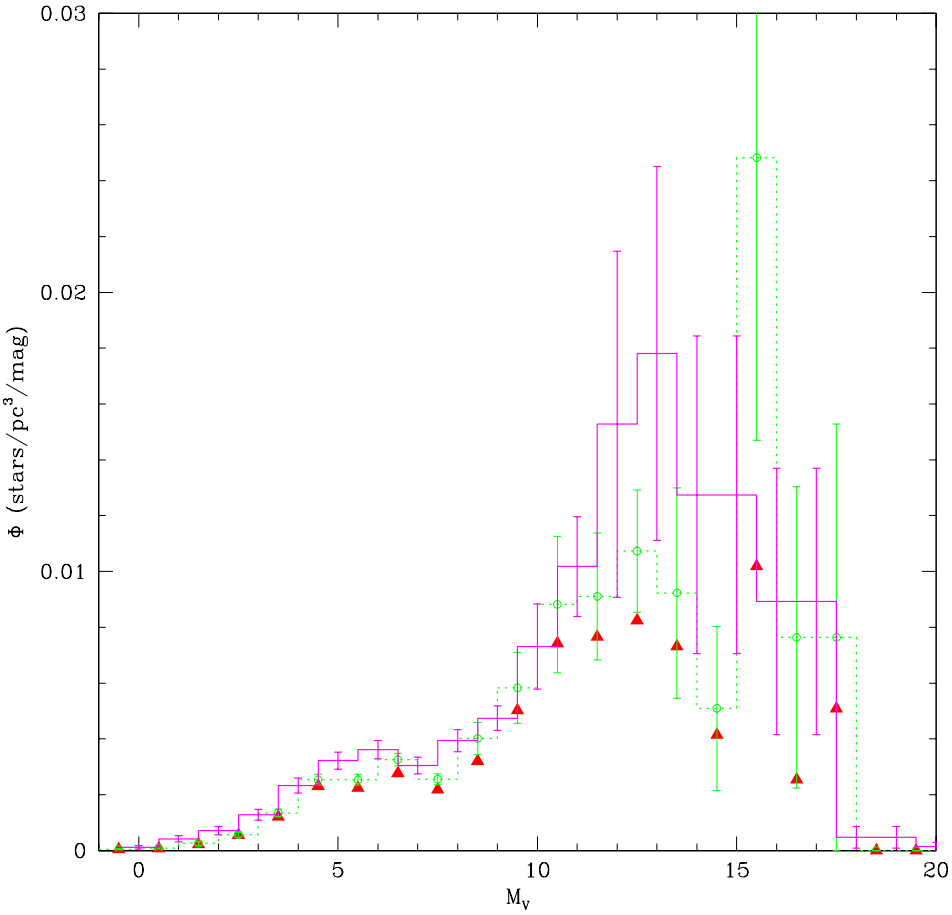

Fig. 8.— The luminosity function for nearby stars, derived by combining data for the Hipparcos 25-parsec sample and the PMSU sample. Data for single stars and primaries are plotted as solid triangles; the open circles plot the space densities once the appropriate companions are included, with the errorbars reflecting Poisson uncertainties. The solid histogram plots $\Phi(M_V)$ from Wielen, Jahreiß & Krüger (1983).

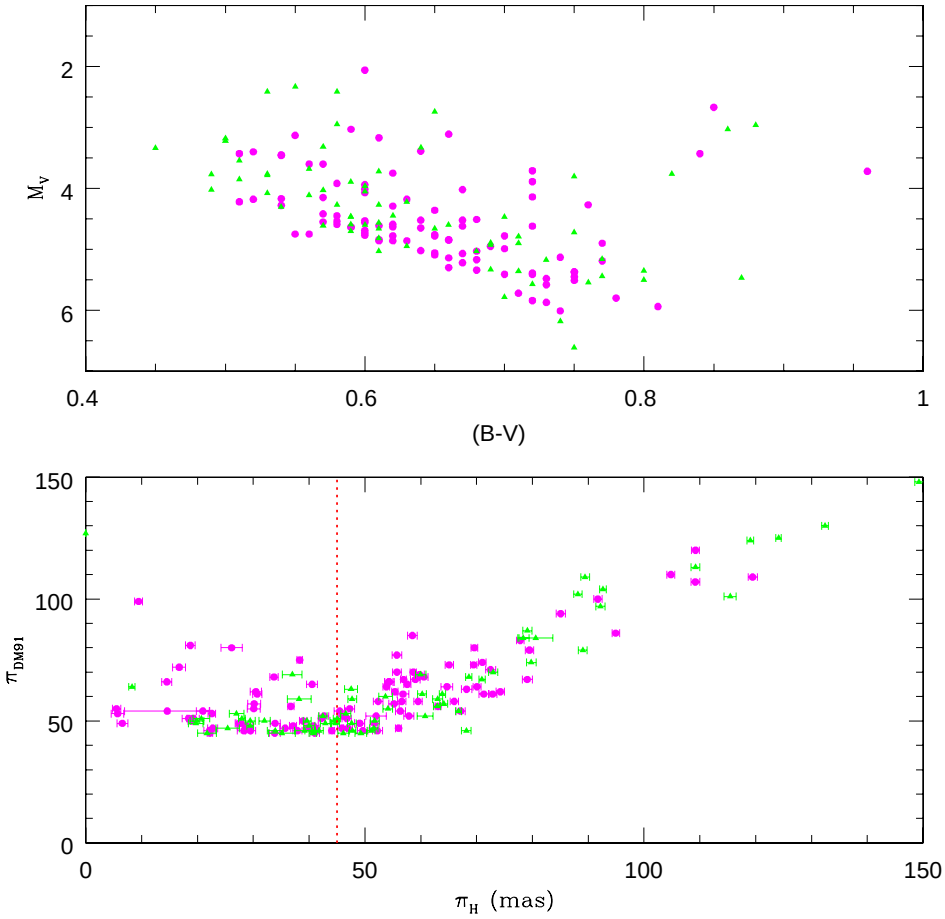

Fig. 9.— The Duquennoy & Mayor G-dwarf sample: the lower figure compares the parallaxes listed in the CNS2 catalogue against the Hipparcos data; the upper figure plots the distribution of the stars in the (M_V, (B-V)) plane. Single stars are plotted as solid triangles, binaries as open circles. The photometry of the latter stars has been corrected to exclude contributions from secondary components.

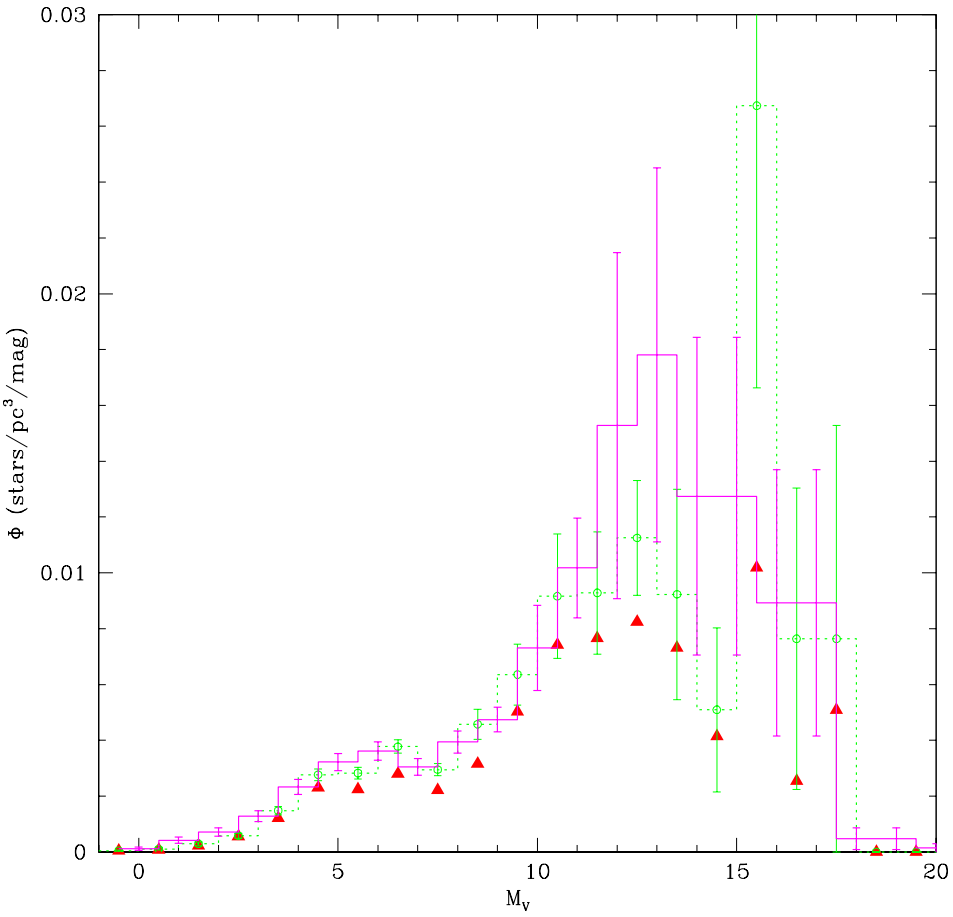

Fig. 10.— The nearby star luminosity function, adjusted to include the contribution from "missing" binary components. The symbols have the same meaning as in Figure 8. As discussed in the text, we have doubled the contribution from known companions to the Hipparcos 25-parsec sample.

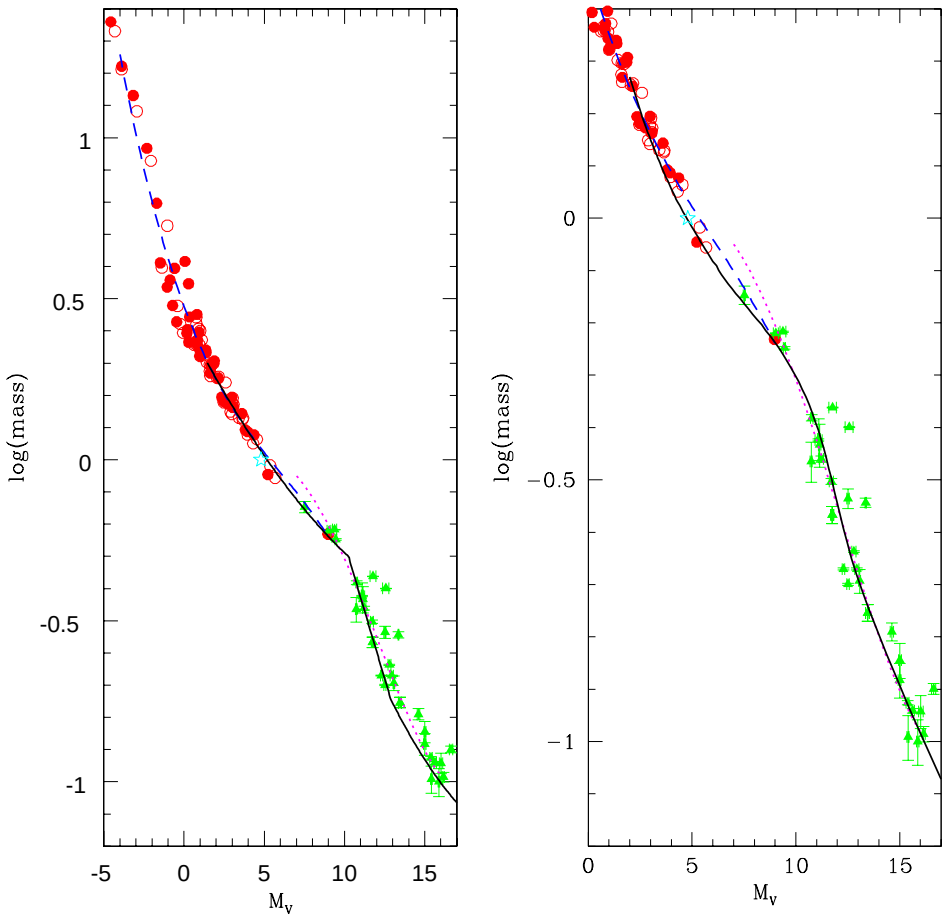

Fig. 11.— The (M_V, mass) relation for main-sequence stars: solid points and open circles plot data for primary and secondary stars, respectively, from Andersen's compilation of eclipsing binaries; solid triangles plot data for lower main-sequence binaries from Ségresan *et al.* (2000). The five-point star marks the Sun. In the left-hand panel, the long-dashed line shows the empirical fit to the upper main-sequence stars given in the text, the dotted line plots the (M_V, mass) relation derived by Delfosse *et al.* (2000) and the solid line shows the three-component fit from Henry *et al.* (1993). Ther right-hand panel compares the former two relations against the KTG semi-empirical relation (solid line).

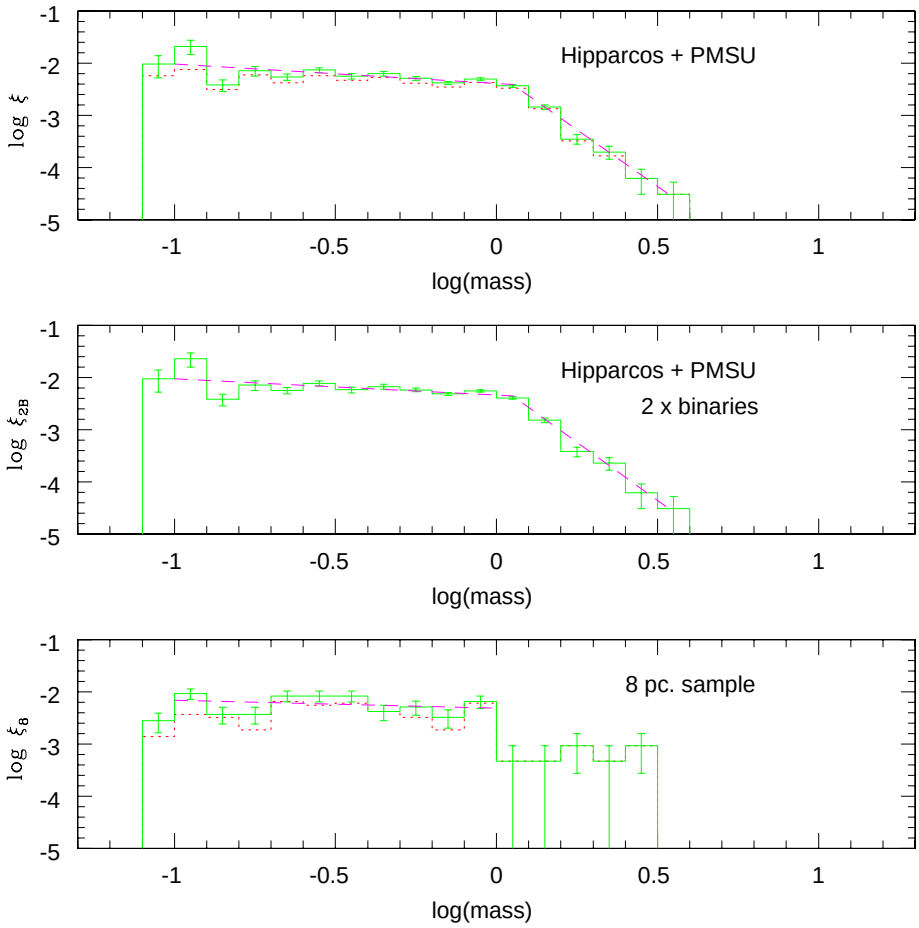

Fig. 12.— The stellar mass function for the Solar Neighbourhood. The uppermost panel shows the results of applying the mass-luminosity relation to the dataset used to derive $\Phi(M_V)$) plotted in Figure 8, with the dotted histogram outlining the contribution from single stars and primary stars in binary systems; the middle panel shows $\xi(M)$ when double weight is given to the Hipparos 25-parsec secondaries; the lowest panel shows $\xi(M)$ for the northern 8-parsec sample (Reid *et al.*, 1999). In each case, the dashed lines plot the best-fit power-law (see text).

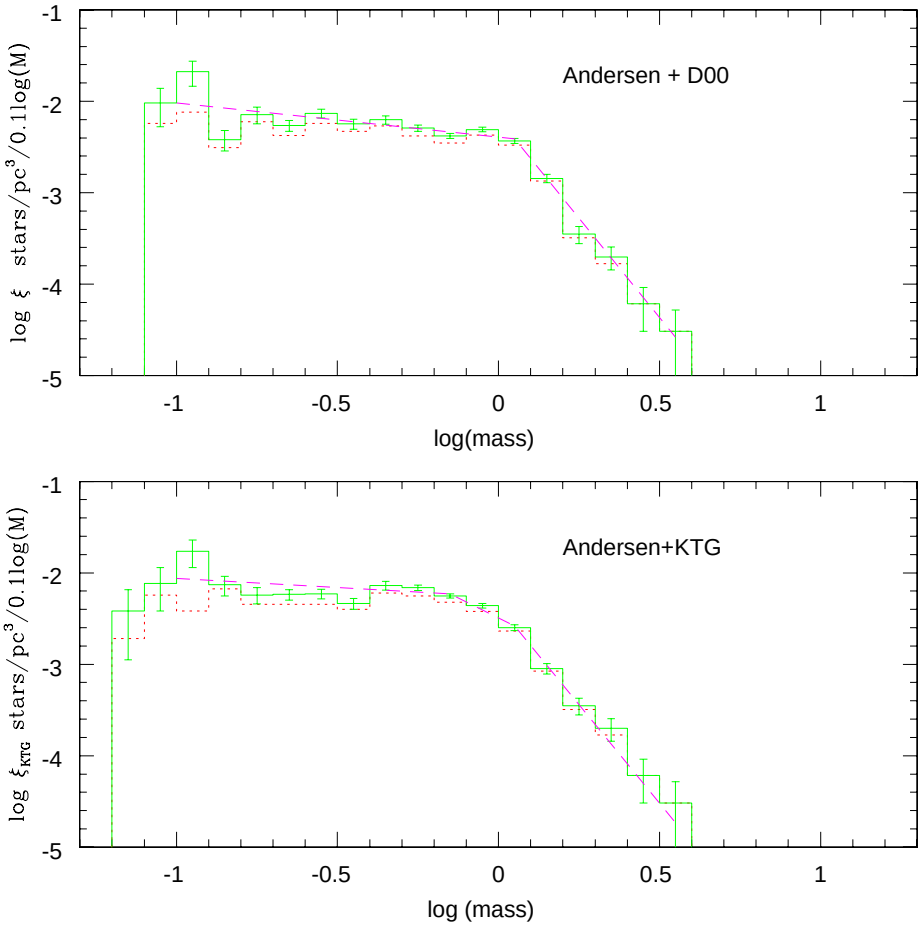

Fig. 13.— A comparison betweenthe present-day mass function derived using the empirical mass-M_V calibration (upper panel) and the KTG semi-empirical calibration (lower panel). The latter includes the empirical eclipsing-binary relation for $M_V < 3.5$. As in Figure 12, the dotted histogram plots results for single stars/primaries. The main differences lie at near-solar masses, with the semi-empirical calibration showing a steepening at $\sim 0.7 M_\odot$ rather than $\sim 1 M_|odot$.

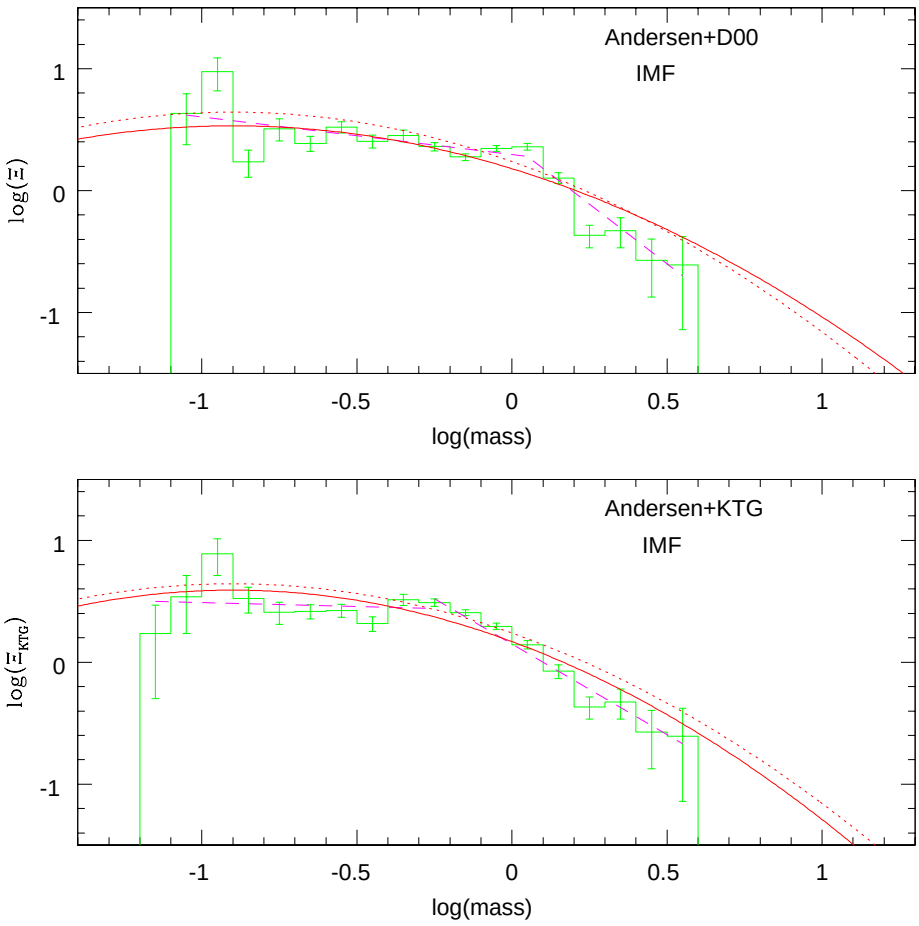

Fig. 14.— The initial mass function: the upper panel shows results based on the empirical mass-M_V relation; the lower plots results using the KTG semi-empirical relation at $M_V > 3.5$. The units on the ordinate are surface density, with an arbitrary normalisation. The dashed lines mark the power-law representations described in the text. The solid line and dotted line plot log-normal functions, with the former plotting the best-fit function (see text) and the latter, the original Millar-Scalo function with C_1=1.15.

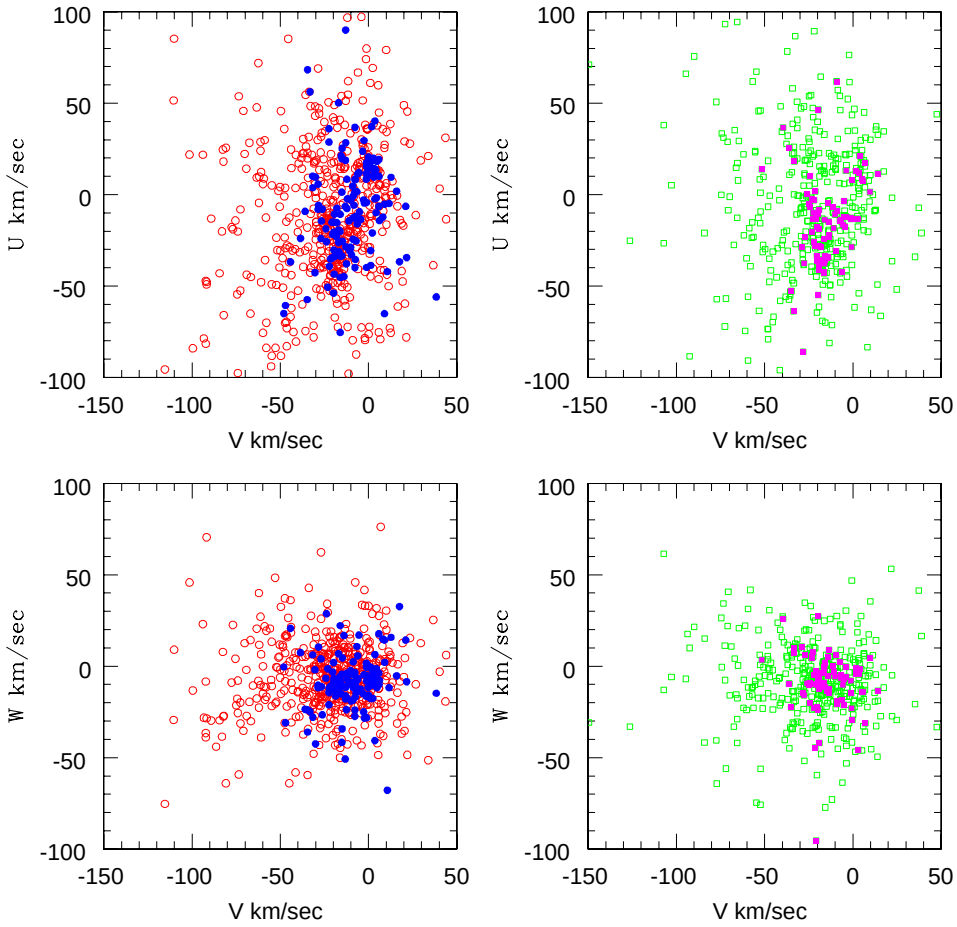

Fig. 15.— (U, V, W) diagrams for the VC^2 (right-hand panels) and Hipparcos 25-parsec (left-hand panels) datasets. Solid points mark dMe dwarfs in the VC^2 sample and Hipparcos stars with $M_V < 4.0$, respectively.

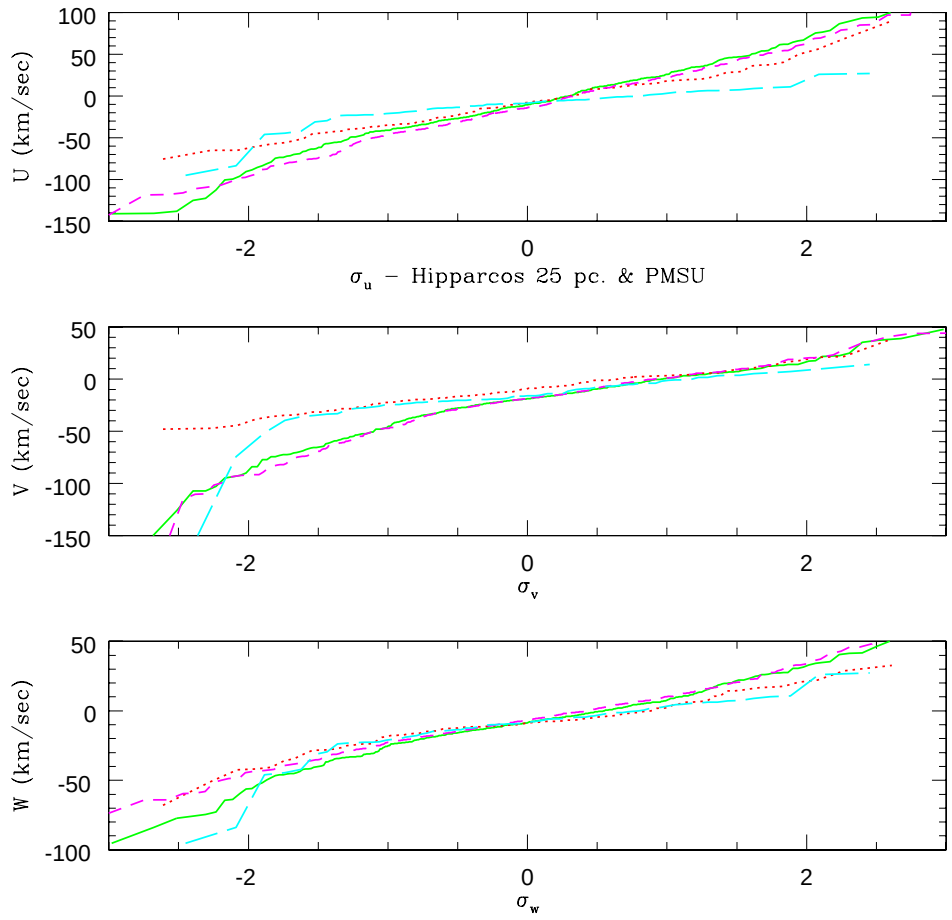

Fig. 16.— Probability plots for (U, V, W) velocity distributions. The solid line plots data for the full VC^2 sample; the long-dashed lines outline data for the 83 dmE dwarfs in the VC^2 sample; the dotted lines plot the distributions of the Hipparcos faint ($M_V > 4$) sample; and the short-dashed lines plot the bright ($M_V \leq 4$) Hipparcos dataset. The similarity between the full VC^2 and faint Hipparcos datasets is clear.

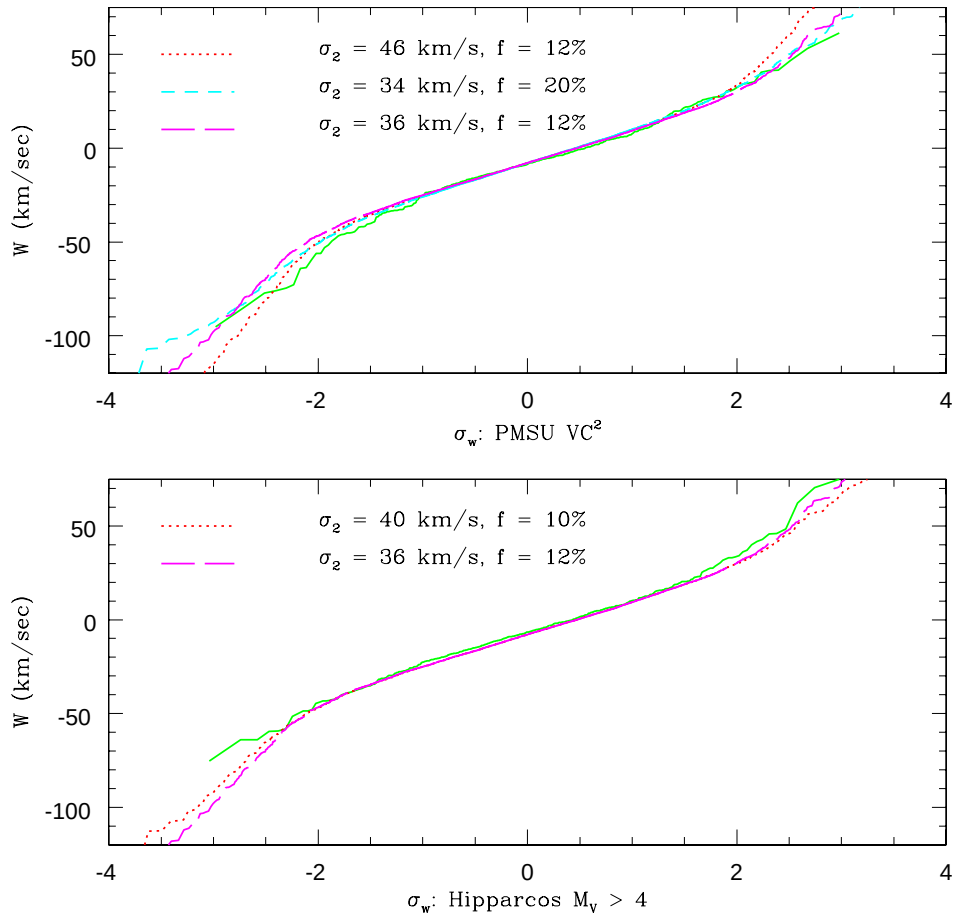

Fig. 17.— Two-component fits to probability plots of the W velocity distribution of the PMSU VC^2 M dwarf sample (upper plot) and the Hipparcos faint-star sample (lower plot). In both cases, the observations are plotted as a solid line and the low-velocity component is modelled with $\sigma_W = 16$ km s^{-1} ; the tabulated velocity distributions and relative normalisations refer to the higher-velocity component.

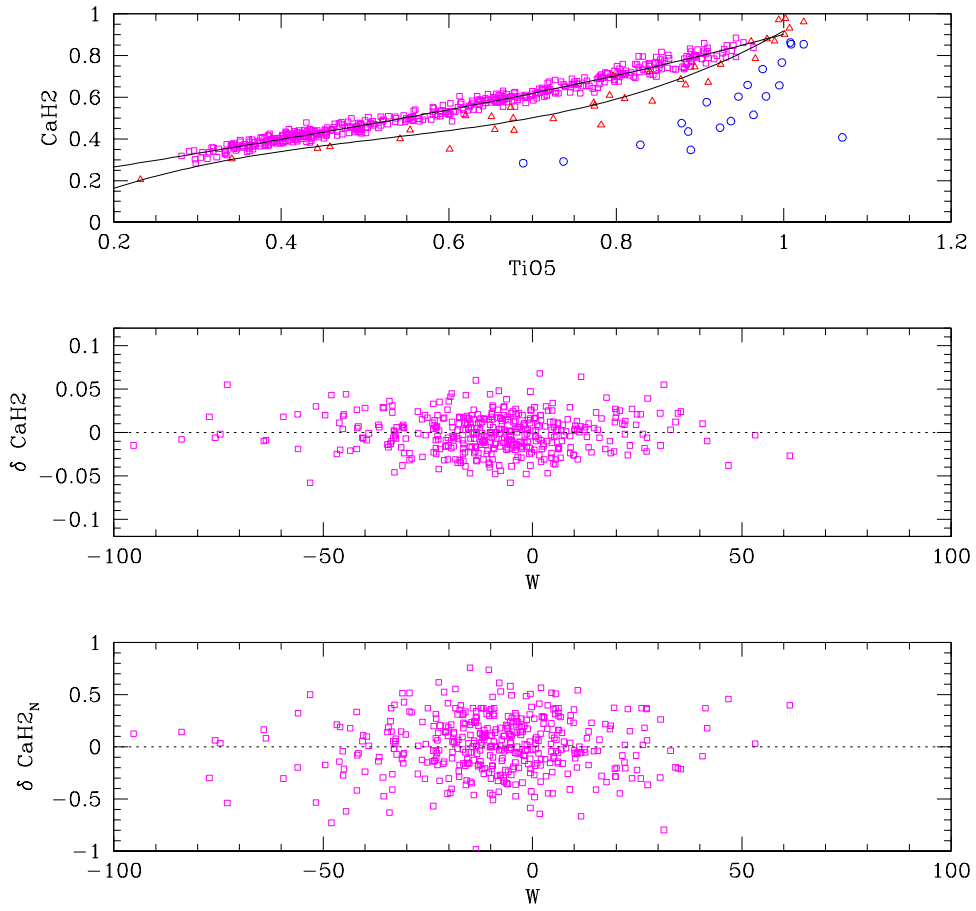

Fig. 18.— The uppermost panel plots the CaH2/TiO5 distribution of the VC[2] M dwarfs (squares), intermediate subdwarfs (sdM - triangles), and extreme subdwarf (esdM - open circles). The solid lines are polynomial relations matched to the first two datasets. The middle panel plots the CaH2 residuals for the VC[2] dwarfs as a function of W velocity; the lower panel plots those residuals normalised to the offset between the mean M dwarf and sdM relations. Neither of the residual plots show evidence for a systematics trend with velocity.